Ab initio theory of planetary materials

Artem R. Oganov*,I, G. David PriceII and Sandro ScandoloIII

I Laboratory of Crystallography, Department of Materials, ETH Hönggerberg, Wolfgang-Pauli-Strasse 10, 8093 Zurich, Switzerland
II Department of Earth Sciences, University College London, Gower St., London WC1E 6BT, UK
III The Abdus Salam International Centre for Theoretical Physics (ICTP) and INFM/Democritos National Simulation Center, 34014 Trieste, Italy

Received November 3, 2004; accepted December 6, 2004

First-principles simulations / Phase diagram / Earth's core / D″ layer / Lower mantle / Computational crystallography

Abstract. *Ab initio* simulations play an increasingly important role in the studies of deep planetary interiors. Here we review the current state of this field, concentrating on studies of the materials of the Earth's deep interior ($MgO-SiO_2-FeO-Al_2O_3$, Fe–Si–S–O) and of the interiors of giant planets (H–He system, $H_2O-CH_4-NH_3$ system). In particular, novel phases and phase diagrams, insights into structural and electronic phase transitions, melting curves, thermoelasticity and the effects of impurities on physical properties of planet-forming materials are discussed.

1. Introduction

Physical processes at planetary surfaces intimately depend on the state of matter at the high pressures and temperatures existing within these bodies. Experimental and computational studies of planet-forming materials play an important role in modelling planetary interiors and enable a deeper physical understanding of planetary processes. Computational studies, which we review here, have the advantage that they can be performed even at those extreme $P - T$ conditions where direct experiments are not feasible. Before reviewing such studies we give a very brief introduction to the physics of the Earth and giant planets (Jupiter, Saturn, Uranus and Neptune), referring the reader to an excellent book [1] for more details.

Internal structure

For the Earth, there is abundant geological evidence and robust seismological models (e.g., the Preliminary Reference Earth Model (PREM) – [2]), which give shear and compressional seismic wave velocities (v_S and v_P, respectively) density (ϱ), and pressure (P) as a function of depth. Seismic tomography gives 3D-variations of seismic wave velocities in the mantle (e.g., Masters et al., 2000), which can in principle be translated into variations of composition and temperature (see [3, 4] for some of the first works).

The available information on giant planets is very limited: we know their masses, sizes, gravitational multipole moments, magnetic field strengths, luminosities, and the compositions of their atmospheres (see, e.g., [1]). Evolutionary models of these planets suggest that they may have

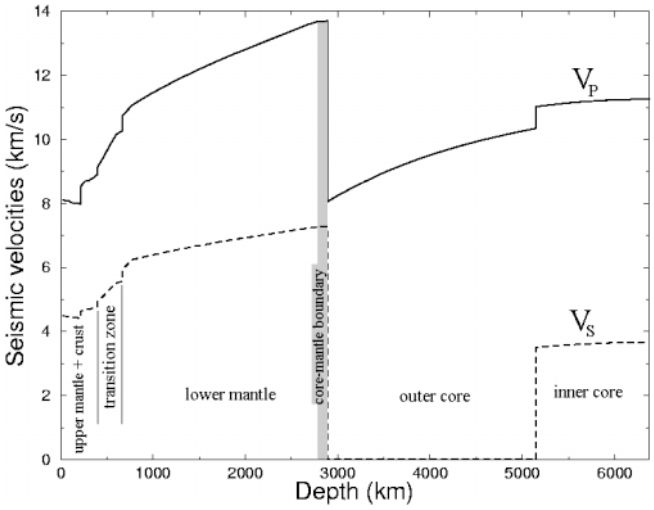

Fig. 1. PREM seismic profile of the Earth. Anomalous core-mantle boundary D″ layer is shown in grey.

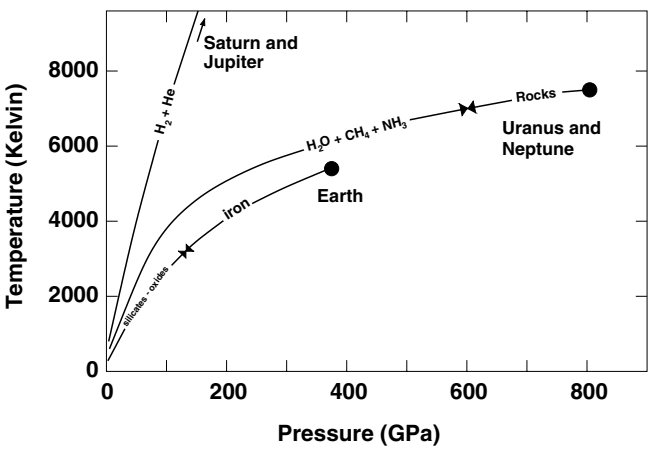

Fig. 2. Pressure – temperature profiles inside the planets of the solar system (adapted from [5]).

* Correspondence author (e-mail: a.oganov@mat.ethz.ch)

"rocky" cores weighing 1–15 Earth-masses, which in the early stages of planetary history triggered a gravitational instability in the surrounding gas clouds and condensation of a predominantly hydrogen-helium mixture in Jupiter and Saturn and a $CH_4-NH_3-H_2O$ mixture in Uranus and Neptune. Giant planets do not have surfaces – their atmospheres gradually become dense fluids (which comprise the largest part of these bodies). Boundaries between different regions (e.g., "molecular" and "metallic" layers in Jupiter and Saturn) may also be gradual – in contrast to the sharp seismic boundaries within the Earth (Fig. 1). Fig. 2 summarises the present knowledge of the pressure-temperature relations and the composition of these planets.

Chemistry

The composition of the Earth is believed to be close to that of a devolatilised chondritic meteorite (Table 1), but there are many uncertainties: first of all, there are many versions of the "chondritic" model (see, e.g., [7, 9]); secondly, chondritic models may be just a first approximation, as some ratios (notably the Mg/Si ratio – where the Earth may be depleted in Si relative to chondrite) seem to depart from chondritic values.

Velocity-density systematics (Birch's law) and elemental abundances suggest that the mantle consists mainly of Mg-silicates with the average atomic number $\bar{M} = 21.3$ [10], which when compared with $\bar{M} = 20.12$ for $MgSiO_3$, 20.15 for MgO, and 20.13 for Mg_2SiO_4, implies ~10% substitution of Mg by Fe. By similar arguments, the core is an Fe-rich alloy: for the liquid outer core Birch's law gives $\bar{M} = 49.3$ (Poirier, 2000) (*cf* the atomic mass of Fe which equals 55.8) implying the presence of 10 wt.% of lighter alloying elements; the inner core is solid, probably crystallising from the liquid outer core.

For Jupiter and Saturn, the main components are H and He with the expected ratio $[He/(H + He)]_{prim} = 0.280 \pm 0.005$ by mass [11]. This is different from the measured atmospheric compositions: $[He/(H + He)]_{Jupiter,\ atmosphere} = 0.238 \pm 0.007$ by mass [12]. The analogous ratio for Saturn is probably still lower: $[H/(H + He)]_{Saturn,\ atmosphere} = 0.18–0.25$ by mass [13]. Perhaps, the most likely explanation of the differences between these numbers and the solar value is the unmixing in the H–He system at planetary conditions – this can be viewed as a "rain-out" of the denser He into the interiors of planets. The H–He mixture is also present on Uranus and Neptune, but comprises only their atmospheres, the major parts of these planets consisting of a $H_2O-NH_3-CH_4$ mixture in the molar proportion 56 : 8 : 36.

Energetics

The energetics of the Earth has been a topic of great and long-standing interest. The main source of the Earth's heat is presently the radioactive decay of U, Th, and ^{40}K, but in the past the gravitational separation of the core and other factors were of importance. The present-day heat flux from the surface of the Earth is 40–44 TW [14] – this, together with the energy needed to maintain the core dynamo, is balanced by radiogenic heat generation, by cooling of the Earth's interior, and possibly also by the crystallisation of the inner core. An understanding of the precise balance of these contributions is needed to understand the dynamics of the Earth and the age of the inner core. Uncertainties still exist however, as for example, under high pressure K becomes a *d*-element, which might facilitate its fractionation into the core – thus creating an important source of radiogenic energy (radioactive ^{40}K isotope) within the core.

For giant planets the main source of heat generation is almost certainly gravitational. In Jupiter and Saturn this would be the gravitational sinking of He. In Neptune (and possibly Uranus, although the heat flux from Uranus is much smaller – [15]) the energy source might be the gravitational energy released at sinking of diamond produced by decomposition of CH_4 at high pressures and temperatures.

Magnetic fields

All planetary magnetic fields are generated by convection of electrically conducting layers inside the planets – the metallic Fe-rich outer core of the Earth, fluid metallic hydrogen inside Jupiter and Saturn, ionically conducting fluid $H_2O-NH_3-CH_4$ system in Uranus and Neptune. The magnetic fields of the latter planets are very eccentric and much weaker than Jupiter's and Saturn's. An illuminating discussion of these "strange" magnetic fields was given in [16].

Table 1. Abundances of some chemical elements (in atoms per 1 atom Si).

Element	The Universe [6]	Whole Earth [7]	Earth's Crust [7]	Upper Mantle [7]	Lower Mantle [7]	Pyrolitic Homogeneous Mantle [8]
O	20.10	3.73	2.9	3.63	3.63	3.68
Na	0.06	0.06	0.12	0.03	$2 \cdot 10^{-3}$	0.02
Mg	1.08	1.06	0.09	0.97	1.09	1.24
Al	0.08	0.09	0.36	0.17	0.06	0.12
Si	1	1	1	1	1	1
S	0.52	–	$8 \cdot 10^{-4}$	$6 \cdot 10^{-4}$	$5 \cdot 10^{-5}$	$2 \cdot 10^{-3}$
Ca	0.06	0.06	0.14	0.12	0.05	0.09
Fe	0.9	0.9	0.11	0.14	0.14	0.16
Ni	0.05	–	$3 \cdot 10^{-5}$	$3 \cdot 10^{-3}$	$4 \cdot 10^{-3}$	$3 \cdot 10^{-5}$

Dynamics

Convection is the predominant mode of dynamics and heat transport inside planets. In the Earth, the outer core and mantle are separately convecting (it might be that the mantle convects as two or more separate systems, or as a single system with an internal barrier at 670 km), and their boundary is a thermal boundary across which heat is transported mainly by conduction. Mantle convection is the physical mechanism behind plate tectonics. Giant planets are characterised by very vigorous convection, perhaps with the exception of Uranus, where convection seems to be hindered.

For a convecting system like the mantle and outer core, the average temperature increases with depth adiabatically (fast convection) or superadiabatically (slow convection). The adiabatic compression law is:

$$\left(\frac{\partial \ln T}{\partial \ln \varrho}\right)_S = \gamma \qquad (1)$$

where T, ϱ and γ are the temperature, density, and the Grüneisen parameter, respectively.

2. Earth's interior

2.1 Lower mantle ($P = 24–136$ GPa, $T = 1600–4200$ K)

Mineralogy of the Earth's mantle has been reviewed in [17]. The traditional pyrolite model includes ~75 vol% $(Mg,Fe)SiO_3$ perovskite, ~20% magnesiowüstite $(Mg,Fe)O$[1], ~5% $CaSiO_3$ perovskite. Other relevant materials include SiO_2 and Al_2O_3 polymorphs, FeO, and various aluminous phases. Recently, it was discovered that at conditions of the D″ layer (i.e. lowermost ~150 km of the mantle), a post-perovskite phase of $MgSiO_3$ with the layered $CaIrO_3$-type structure is stable [18, 19].

Periclase (MgO)

At ambient conditions MgO crystallises in the NaCl ("B1") structure that type, which is remarkably stable: this is the only structure that has ever been observed for MgO, although experiments have explored pressures up to 227 GPa [20] and all the way up to the melting temperature. It is expected that under extreme pressure the CsCl-type ("B2") structure will become stable, but the best theoretical calculations [21–25] indicate that the pressure of such a transition is very high, ~510 GPa.

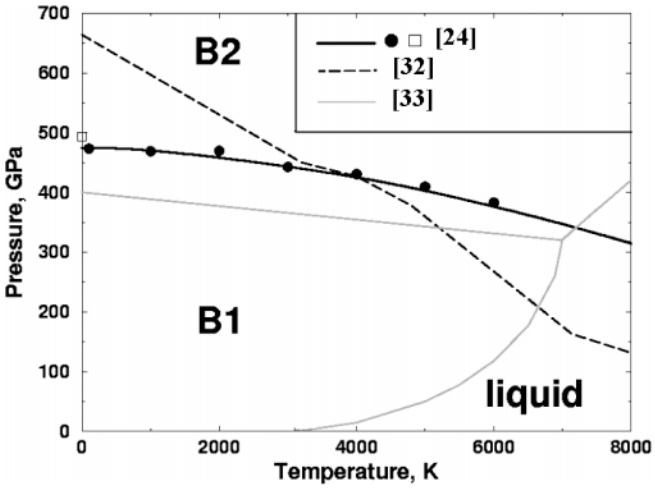

Fig. 3. Phase diagram of MgO (adapted from [24]). Calculations [24]: *solid black line* – result of integration of the Clapeyron slopes, *solid circles* – direct calculations, *open square* – static transition pressure.

Table 2 gives a summary of the calculated properties (lattice parameter and volume, bulk modulus and its pressure derivatives, B1–B2 transition pressure (P_{tr}), dielectric constants, heat capacity, and entropy) of MgO in comparison with experiment, with overall good agreement.

Theory and experiment [25, 28–31] show large departures of the elastic constants from the Cauchy law, indicating the importance of many-body interactions. The B1–B2 phase boundary has been calculated in [24, 32, 33], but only the calculation in [24] was fully *ab initio*, performed within density-functional perturbation theory [34, 35]. The resulting phase diagram (Fig. 3) shows that at all conditions of the Earth's interior MgO has the NaCl ("B1") structure.

Fig. 4 shows the calculated [24] phonon dispersion curves for MgO; the agreement with experiment is excellent. These lattice-dynamical calculations showed that zero-point energy would lower the B1–B2 transition pressure by 16 GPa, an unusually large correction. According to the calculations, the B2 phase is dynamically unstable at all pressures below 110 GPa. This means that this phase, when synthesised in its stability field, cannot be decompressed to a pressure lower than 110 GPa – as at lower pressures it would spontaneously transform back into the NaCl-structured phase.

In the lower mantle MgO will contain some 10–20 mol% Fe. It has been shown experimentally [36] that between 60–70 GPa magnesiowüstite $(Mg_{0.83},Fe_{0.17})O$ undergoes a transition associated with high-spin to the low-

[1] In high-pressure literature this phase is commonly called magnesiowüstite (or, sometimes, ferropericlase), while it would be more correct to call it "Fe-bearing periclase". Here, we follow the more common notation.

Table 2. Physical properties of MgO (B1 structure).

	a_0, Å	K_0, GPa	K_0'	K_0'', GPa^{-1}	P_{tr}, GPa	ε_∞	ε_0	C_V (300 K), J mol^{-1}K^{-1}	S (300 K), J mol^{-1}K^{-1}
LDA [24]	4.240	172.6	4.004	−0.025	490	3.15	8.87	36.58	26.81
GGA [25]	4.253	150.6	4.103	(−0.027)	509	–	–	–	–
Exp.	4.212	160.2 [26]	3.99 [26]	(−0.024) [26]	>227 [20]	2.95	9.64	36.87 [27]	27.13 [27]

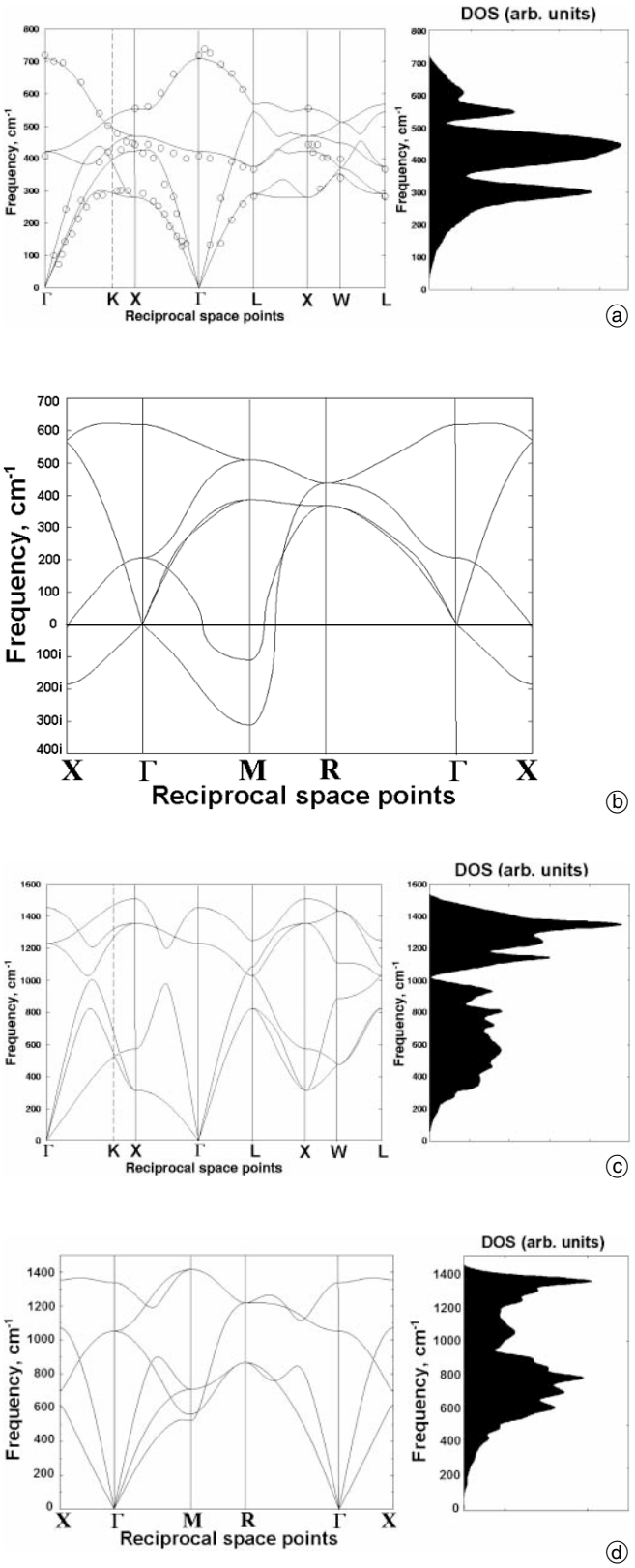

Fig. 4. Phonon dispersion curves at 0 GPa in (**a**) B1-structured and (**b**) B2-structured MgO and at 600 GPa in (**c**) B1 phase and (**d**) B2 phase (taken from [24]).

spin transition of Fe^{2+} ions. This transition could have a large effect on the elastic properties and could cause a seismic discontinuity within the lower mantle. Disproportionation of (Mg,Fe)O has been claimed in some experiments [37], but was not seen in others [38].

SiO_2 polymorphs

It is well established that stishovite, a rutile-structured phase stable above 8 GPa, becomes mechanically unstable at ∼50 GPa and, through a second-order transition, distorts into an orthorhombic $CaCl_2$-structured phase [39–49]. At ∼90 GPa the α-PbO_2 structure polymorph becomes stable [41–43, 46, 49–51]. The sequence of phase transformations stishovite – $CaCl_2$ structure – α-PbO_2 structure reveals the tendency towards more geometrically regular close packing of the component anions. However, according to theoretical predictions [41–43, 49], a phase with the pyrite structure becomes thermodynamically stable at ∼210 GPa; this structure cannot be described as being based on a close packing of spherical anions, yet it is very dense (compared with the close-packed α-PbO_2 structure, it is 4.6% denser at 0 GPa and 3.2% denser at the transition pressure). The name "pyrite structure" is rather nominal in this case: the "dumbbell" O–O distances are quite long, perhaps too long to be counted as true bonds, 2.385 Å at 0 GPa and 2.043 Å at 260 GPa. Analogous pyrite-type structures have been experimentally found at high pressure in SnO_2, RuO_2, PbO_2 [52] and GeO_2 [53]. Topological analysis of electron density [54] shows that SiO_2 phases are significantly ionic (zero-pres-

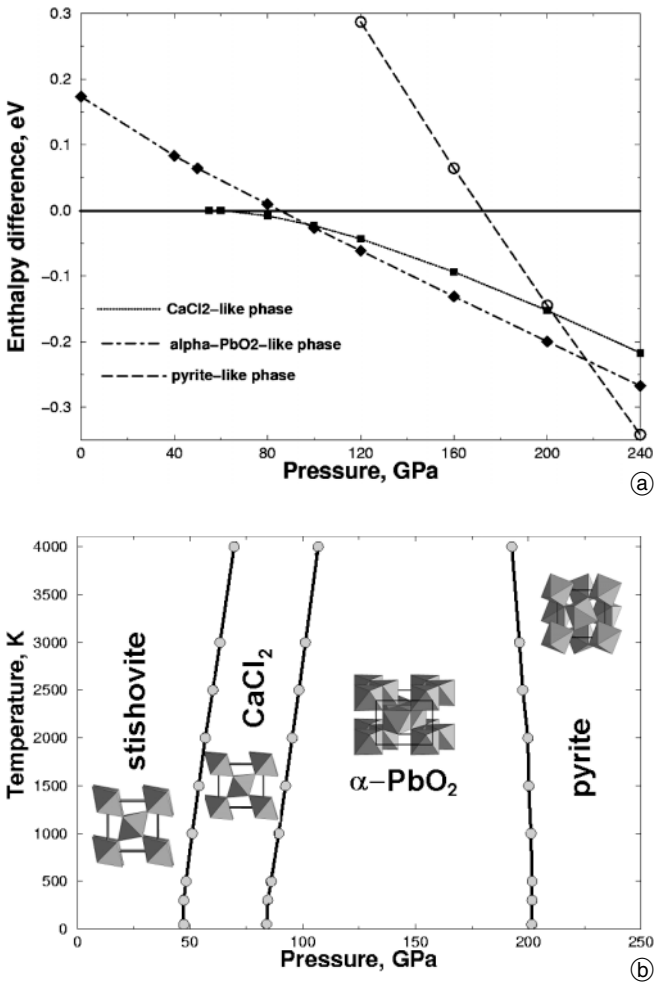

Fig. 5. High-pressure phases of SiO_2: (**a**) Enthalpy (relative to stishovite, per formula unit) all-electron PAW calculations, GGA; (**b**) Theoretical phase diagram [49], pseudopotential LDA calculations.

sure charges of Si are: +3.23 in stishovite,[2] +3.20 in the α-PbO_2-like phase, and +3.17 in the pyrite-type phase) [49]. The relative enthalpies of the different phases and the calculated phase diagram are shown in Fig. 5.

Al_2O_3 polymorphs

Both theoretical [56–58] and experimental [59, 60] work has demonstrated that at 80–100 GPa Al_2O_3 transforms from the corundum structure into the Rh_2O_3(II) structure (Fig. 6). This transition, just like the α-PbO_2 – pyrite structure transition in SiO_2, shows a breakdown of anion close packing at high pressure. Close packing can be violated when electronic transitions occur or when coordination numbers of cations become incompatible with close-packed anion arrangements, which have only 2-, 3-, 4-, and 6-coordinated sites. However, none of these phenomena take place in SiO_2 and Al_2O_3. One could speculate that in the high-pressure phases of SiO_2 and Al_2O_3 anions are no longer spherical and therefore ideas of close packing of spheres are irrelevant. Irregular shapes of atoms (which can be defined in Bader theory – [54]) are energetically expensive, but can result in a higher density – and it is the crystal density that ultimately determines the high-pressure structural stability. The high pressure behaviour of Al_2O_3 and SiO_2 show the limitations of the traditionally widely applied principle of close packing of spheres. Above 130 GPa, Al_2O_3 adopts a $CaIrO_3$-type structure, isotypical with that of post-perovskite phase of $MgSiO_3$ [58].

Al_2SiO_5 polymorphs

It had been claimed [61] that at high temperatures and pressures a V_3O_5-like phase of Al_2SiO_5 (where both Al and Si are in the octahedral coordination, see Fig. 7) becomes stable and that this phase would be the main Al-containing mineral in the lower mantle, however subsequent experimental [62] and theoretical [63] studies found that Al_2SiO_5 polymorphs break down into the mixture of Al_2O_3 and SiO_2 above ~10 GPa.

In the Earth, it is most probable that Al is hidden in $MgSiO_3$ perovskite[3] as an impurity [71], though in Al-rich subducted slabs individual aluminous phases cannot be ruled out – such as $MgAl_2O_4$ in the $CaFe_2O_4$ and $CaTi_2O_4$ structures [72, 73], or a hollandite-type modification of $(Ca,Mg)Al_2Si_2O_8$ [74].

Metastable compression of sillimanite and andalusite to 38 GPa and 52 GPa, respectively, was predicted to lead to interesting new metastable phases [75]: amorphisation was predicted for andalusite, and an isosymmetric transition for sillimanite. The metasable isosymmetric transition in

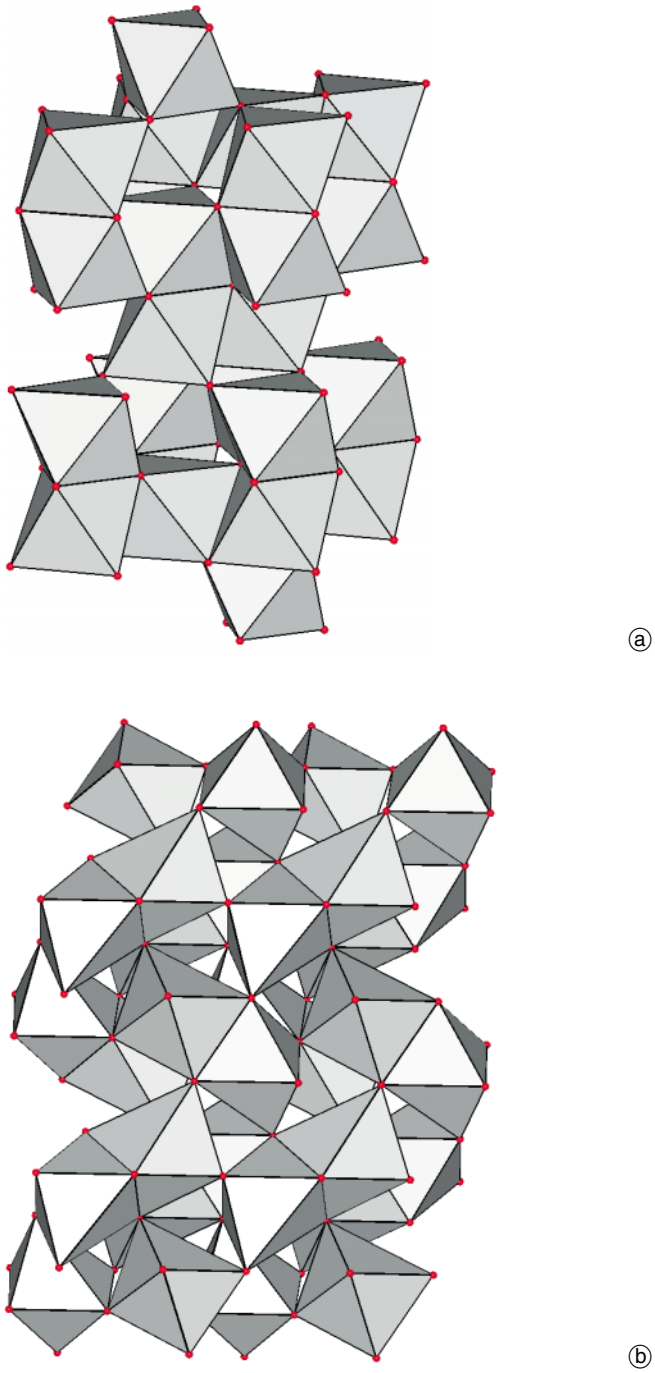

Fig. 6. Structure types of (**a**) corundum and (**b**) Rh_2O_3(II).

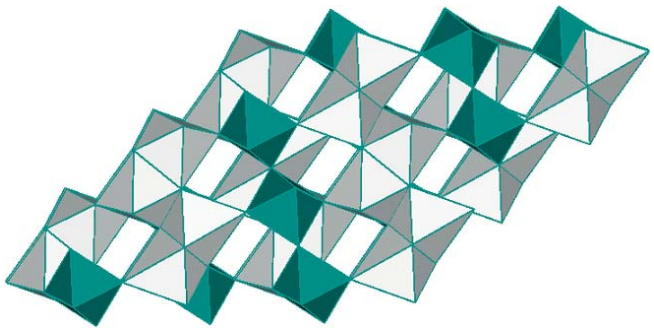

Fig. 7. Hypothetical V_3O_5-like phase of Al_2SiO_5 (from [63]).

[2] Kirfel et al. [55] found the following Bader charges in stishovite: +3.39 (Si) and −1.69 (O) from experimental charge densities and +3.30 (Si) and −1.65 (O) from GGA calculations (our numbers were based on LDA densities).

[3] The expected ~5–10 mol% of Al impurities in perovskite can have a significant effect on the partitioning of Fe between perovskite and magnesiowüstite [64], probably due to coupled Al^{3+}–Fe^{3+} substitutions in the perovskite structure [65, 66]. The effect of Al impurities on the compressibility of perovskite is still an open question [67–70].

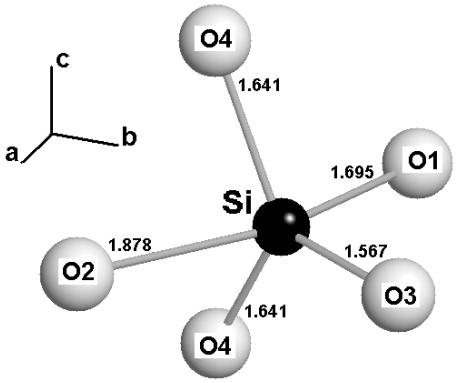

Fig. 8. Geometry of the SiO_5 polyhedra in the post-sillimanite structure at 50 GPa [75].

sillimanite (both phases have *Pbnm* symmetry) was predicted to be first order, reversible with a hysteresis, and with the high-pressure phase having Si atoms and half of the Al atoms in the 5-fold coordination (Fig. 8).

FeO

Despite its apparent simplicity, FeO is currently one of the most challenging materials for theoretical studies. At low pressures it is always non-stoichiometric (at high pressure non-stoichiometry is believed to be suppressed) and, when cooled below $\sim$200 K its NaCl-type structure antiferromagnetically orders and develops a rhombohedral distortion, measured by the deviation of the primitive cell angle α from 60° (Table 3). FeO is an insulator, but LDA and GGA calculations show a finite density of states at the Fermi level, characteristic of a metal. Moreover, such simulations erroneously predict an antiferromagnetic anti-NiAs structure to be the lowest-energy phase. Different theoretical [76–81] and experimental [82, 83] works on the high spin – low spin transition in the distorted NaCl structure produced very different results. Perhaps the simplest way to treat Mott insulators (such as FeO) is the DFT + U method, its simplest formulation being due to Dudarev et al. [84, 85]. Interestingly, GGA + U calculations give two different solutions for antiferromagnetic FeO – those with the rhombohedral and monoclinic symmetries [81].

$CaSiO_3$ perovskite

For a long time, this mineral was considered to be cubic, but recent high-pressure experiments [88, 89] determined a tetragonal symmetry. While pseudopotential calculations [90, 91] have led to the conclusion that the structure is cubic, all-electron calculations [92–94] (and also a more approximate study [95]) show that the minimum-energy structure is orthorhombic or tetragonal. This could indicate technical problems with earlier pseudopotential calculations – such as poor treatment of semicore states, ghost states problems, etc. – which can be serious for Ca [96, 97]. Although the expected structural distortion in $CaSiO_3$ perovskite is small, the effect on its physical properties could be large: Stixrude et al. [93] even related a tetragonal-cubic transition in $CaSiO_3$ perovskite with a minor seismic discontinuity observed at the 1200 km depth (e.g., [98]).

Table 3. Structure of FeO.

Property	LDA	GGA	Experiment
V_0, Å^3	142.50	155.81	165.20[a]
a_0, GPa	6.277	6.385	6.236[a]
α°	51.9	53.4	58.4[a]
μ_{Fe}	3.09	3.25	3.32 [87]

a: Structural parameters for the rhombohedral cell are extrapolations of data [86] at 90 K.

$MgSiO_3$ perovskite

$MgSiO_3$ perovskite, the mineral dominating the Earth's lower mantle, has been a subject of a number of detailed theoretical and experimental studies. Since the first *ab initio* works on this material [99–102] great progress has been made in theoretical methodology. Both early and later investigations [3, 103, 104] have confirmed that $MgSiO_3$ perovskite has the *Pbnm* symmetry at all conditions of the Earth's mantle. This rules out a cubic ($Pm\bar{3}m$) perovskite phase that was expected to be a superionic electrical conductor [105, 106] due to diffusion of O^{2-} ions. A dynamical "snapshot" of the orthorhombic structure of $MgSiO_3$ perovskite at 88 GPa and 3500 K is shown in Fig. 9.

Orthorhombic $MgSiO_3$ perovskite has been found by most researchers (e.g., [107–109]) to be stable throughout the $P-T$ regime of the lower mantle, but research has been reported suggesting it decomposes into $MgO + SiO_2$ at lower mantle conditions [110]. Such decomposition would have dramatic implications for the structure, dynamics, and chemistry of the mantle. *Ab initio* simulations, however, suggest that perovskite is stable to decomposition at lower mantle $P-T$ conditions, and that both pressure and temperature stabilise it relative to the oxides ([111], see Fig. 10).

Detailed calculations of the elastic constants of $MgSiO_3$ perovskite as a function of pressure [104, 112, 113] and temperature [3, 114, 115] agree well with experimental data [116, 117], and provide reliable information at extreme conditions. These calculations constitute one of the basic sources of information for interpretationing the

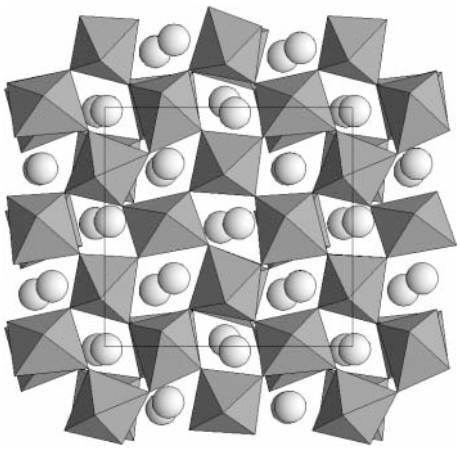

Fig. 9. 'Snapshot' of the crystal structure of $MgSiO_3$ perovskite at 88 GPa and 3500 K from *ab initio* MD simulations [3].

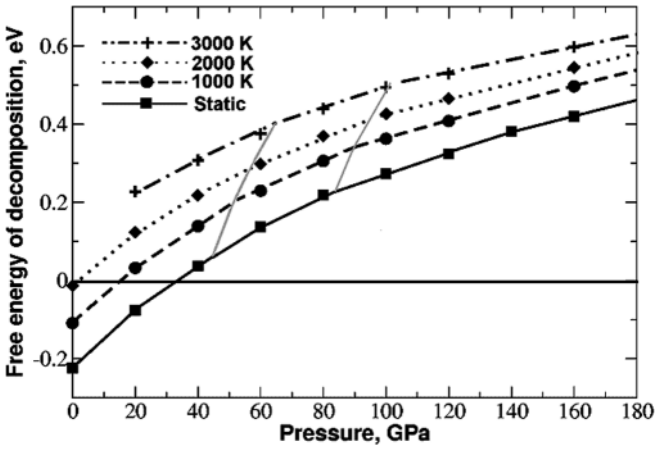

Fig. 10. Gibbs free energy of decomposition of $MgSiO_3$ perovskite [111]. Thin gray lines separate regions of stability of different SiO_2 phases. All lines are guides to the eye.

seismic models of the Earth's lower mantle. The first theoretical determination of the temperature derivatives of seismic wave velocities at lower-mantle pressures and temperatures [3] has also been used for interpreting seismic tomography data in terms of temperature variations in the lower mantle. The results implied large lateral temperature contrasts within the mantle, reaching 2000 K near the core-mantle boundary.

The calculated Grüneisen parameters γ(V) of $MgSiO_3$ perovskite [3, 104] and MgO [25] allowed Oganov et al. [118] to estimate the lower mantle adiabat (Eq. 1), which turned out to be quite similar to the classical geotherms [119, 120]. The resulting thermal model [118] of the lower mantle is shown in Fig. 11.

It can be seen that our maximum mantle temperature matches well an independent estimate of the temperature of the core at the boundary with the mantle [123]. Comparing our temperatures with experimental solidus of pyrolite [124], one can expect some degree of partial melting, restricted only to the hottest regions in the very bottom of the lower mantle. This agrees with seismological observations [125].

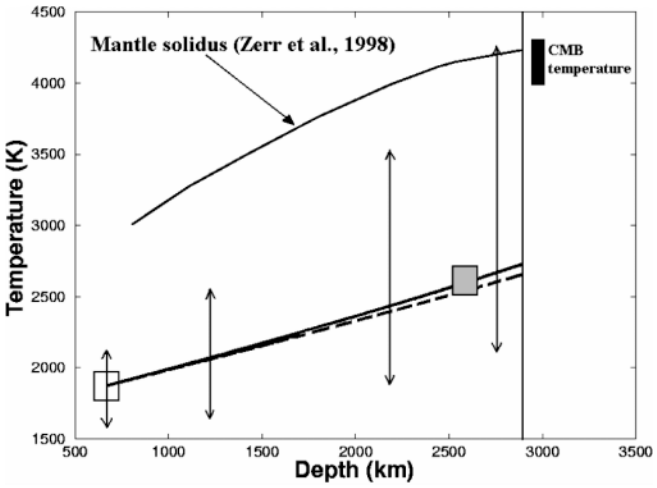

Fig. 11. Schematic temperature distribution in the lower mantle. Two-headed arrows indicate the maximum temperature contrasts (the lower and the upper arrows at each depth give the lowest and the highest temperature, respectively). Solid and dashed lines are adiabats calculated using Grüneisen parameters of $MgSiO_3$ and MgO, respectively: the difference is small, and the geotherm is well constrained between these lines. Open square – datum [121], filled square – datum [122], derived from experimental phase equilibria. Mantle solidus is from the work of Zerr et al. [124].

Post-perovskite $MgSiO_3$: a recent discovery

The lowermost ~150 km of the mantle, the so-called D″ layer, has long been known to show anomalous seismic features, such as strong seismic anisotropy, anticorrelation between bulk and shear seismic wave velocities, and the presence of a seismic discontinuity at top of the D″ layer. These features could not be explained by traditional mineralogical models, and in fact there was geophysical evidence [126] for some phase transition as the cause of the D″ discontinuity. In 2002–2003 S. Ono and colleagues performed important experiments on Fe_2O_3 and found [127] that above 60 GPa iron oxide transforms into a new phase with a $CaIrO_3$-type *Cmcm* layered structure (Fig. 12a). This was very surprising, because layered structures are usually destroyed by high pressure producing framework structures. Since $MgSiO_3$ and

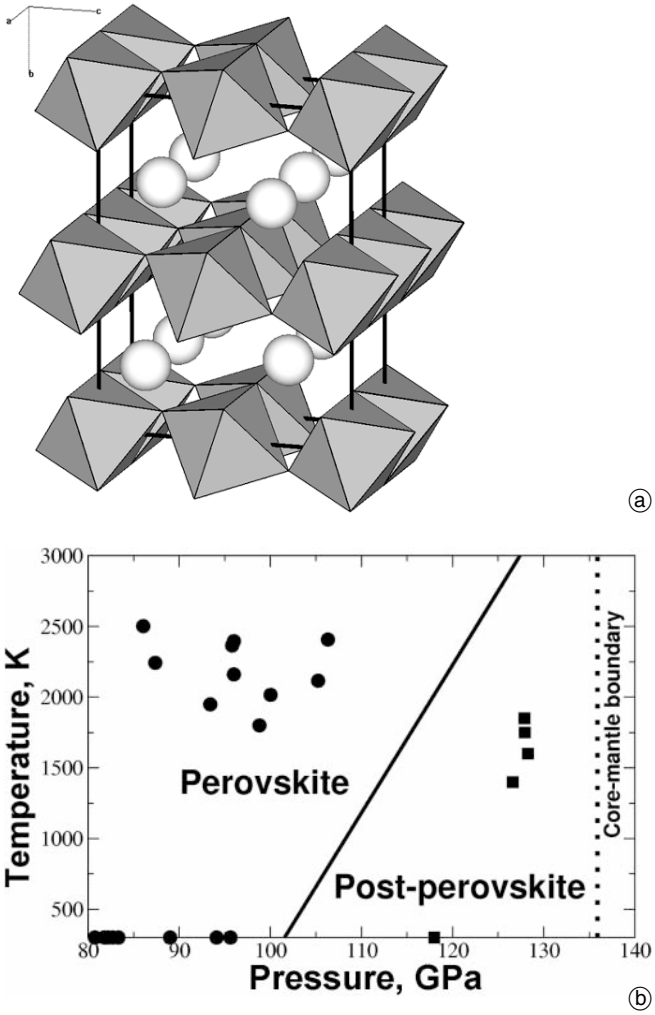

Fig. 12. Crystal structure (**a**) and stability (**b**) of post-perovskite phase of $MgSiO_3$ [18]. Isotypical structures are known for Fe_2O_3, $CaIrO_3$, $FeUS_3$, $PbTlI_3$, $UScS_3$, $KTmI_3$, $AgTaS_3$, $CaInBr_3$. In (b): solid line – theory, symbols – experimental data (squares – post-perovskite phase).

Fe_2O_3 have very similar high pressure behaviour (namely, the sequence of high-pressure phase transitions: corundum-perovskite-$CaIrO_3$), Ono et al. [127] suggested that a $CaIrO_3$-type phase could be stable for $MgSiO_3$ at pressures beyond the perovskite stability field. Subsequently, the new phase of $MgSiO_3$ was found in a joint theoretical and experimental study [18] where the predicted phase diagram (Fig. 12b) guided experimental synthesis (which fully confirmed the calculations). This phase was independently discovered in another experimental study [19]. *Ab initio* calculations of [18] and works that followed the initial discovery of [18, 19] demonstrate that many seismic anomalies known for the D″ layer (at least, the D″ discontinuity and its topography, seismic anisotropy, anomalous v_s/v_ϕ anticorrelation and v_s/v_p correlation) are explained by the elastic properties of the new phase and the large Clapeyron slope (8–10 MPa/K) of the perovskite/post-perovskite equilibrium line.

2.2 CORE ($P = 136$–365 GPa, $T = 4000$–6000 K)

As discussed above, it is well established that the core is an Fe-rich alloy. This is contrary to the interesting hypothesis put forward by W. H. Ramsey in 1949 that the Earth's dense core is not chemically different from the mantle. Rather, he suggested that at high pressure (136–365 GPa in the core) silicates of Mg, Al, and Ca are transformed into ultradense metallic forms. This idea is geochemically not viable, and was not suported by experiments (see [128]) or theoretical calculations (see, e.g., [129]): mantle silicates and oxides remain insulating and never adopt superdense structures or become metallic at the Earth's core conditions. For example, Oganov et al. [24] predicted metallization of MgO at the pressure of 21 TPa (in the CsCl-type structure), more than 50 times higher than the pressure at the centre of the Earth. The calculated valence electron density distribution in that metallic CsCl-structured form of MgO is shown in Fig. 13. Metallization can be viewed as being due to band overlap; in real space it is marked by the large overlap of valence electron densities of the neighbouring oxygen atoms seen in Fig. 13.

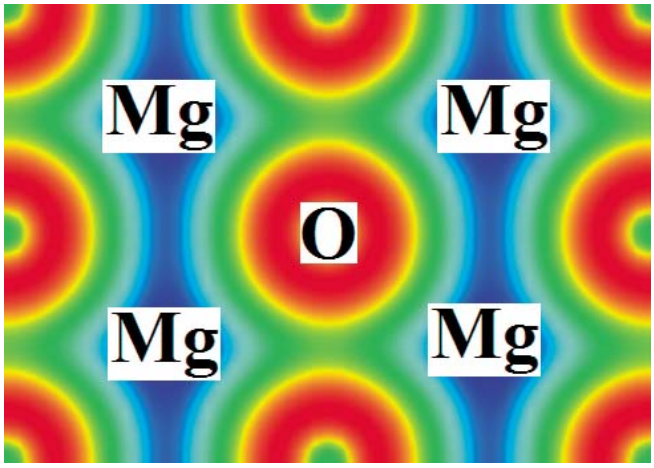

Fig. 13. (110) section of the valence electron density distribution in the CsCl-structured phase after metallisation.

The fact that the core is largely composed of Fe was firmly established as a result of Birch's [130] analysis of mass-density/sound-wave velocity systematics. Today we believe that the outer core is about 6 to 10% less dense than pure liquid Fe, while the solid inner core is a few percent less dense than crystalline Fe [131]. From cosmochemical and other considerations, it has been suggested [132–134] that the alloying elements in the core might include S, O, Si, H and C. It is also probable that the core contains minor amounts of other elements, such as Ni and K. The exact temperature profile of the core is still controversial [135], but it is generally held that the inner core is crystallising from the outer core as the Earth slowly cools, and that (as a result of the work outlined below) core temperatures are in the range ~4000–5500 K, while the pressure at the centre of the Earth is ~360 GPa.

Before we can even begin to provide a materials based interpretation of the composition and structure of the core, we must understand the behaviour of its primary constituent (Fe) under core conditions. At ambient conditions, Fe is crystalline and has a body-centred cubic (*bcc*) structure. This transforms with temperature to a face centred cubic (*fcc*) form, and with pressure transforms to a hexagonal close packed (*hcp*) phase, ε-Fe. The high *P*/*T* phase diagram of pure iron itself however is still controversial (see the discussions in [136, 137]). Various diamond anvil cell (DAC) based studies have been interpreted as showing that *hcp* Fe transforms at high temperatures to a phase which has variously been described as having a double hexagonal close packed structure (*dhcp*) [138] or an orthorhombically distorted *hcp* structure [139]. Furthermore, high pressure shock experiments have also been interpreted as showing a high pressure solid-solid phase transformation [140, 141], which has been suggested could be due to the development of a *bcc* phase [142]. Other experimentalists, however, have failed to detect such a post-*hcp* phase [143, 144] and have suggested that the previous observations were due either to minor impurities or to metastable, strain-induced behaviour.

Further progress in interpreting the nature and evolution of the core would be severely hindered if the uncertainty concerning the crystal structure of the core's major chemical component remained unresolved. An alternative approach to this problem, however, is to use *ab initio* calculations, which have been shown to provide an accurate means of calculating the properties of materials at high *P* and *T*. Thus, Vočadlo et al. [145] carried out a series of calculations to determine *ab initio* the stable phase of Fe. They performed spin polarized simulations on candidate phases (including a variety of distorted *bcc* and *hcp* structures and the *dhcp* phase) at pressures ranging from 325 to 360 GPa. These revealed, in agreement with Söderlind et al. [146] that at core pressures only *bcc* Fe has a residual magnetic moment and all other phases have zero magnetic moments. Vočadlo et al. [145] found that at core pressures and zero temperature, both the *bcc* and the suggested orthorhombic polymorph of iron are mechanically unstable. The *bcc* phase can be continuously transformed to the *fcc* phase (confirming the findings of [147]), while the orthorhombic phase spontaneously transforms to the *hcp* phase, when allowed to relax to a state of isotropic

stress. In contrast, *hcp*, *dhcp* and *fcc* Fe remain mechanically stable at core pressures, and Vočadlo et al. [145] were therefore able to calculate their phonon frequencies and free energies. They concluded that, on the basis of lattice dynamic calculations over the whole $P-T$ space investigated, the *hcp* phase of Fe has the lowest Gibbs free energy, and is therefore the stable form of Fe under core conditions, indicating that the true phase diagram for Fe is simpler than previously suggested.

The high *P* melting of Fe

Having shown how *ab initio* calculations can be used to establish the sub-solidus phase relations in high P Fe, we now consider its high *P/T* melting behaviour. The temperature distribution in the core is poorly constrained and consequently a reliable estimate of the melting temperature of Fe at the pressure of the inner-core boundary (ICB) would be valuable. There is much controversy over the high P melting behaviour of Fe [155], with estimates of the T_m of Fe at ICB pressures ranging between ~4500 K to ~7500 K.

Since both calculations and recent experiments suggest that Fe melts from the ε-phase in the pressure range immediately above 60 GPa, we focus here on the equilibrium between *hcp* Fe and liquid Fe. The condition for two phases to be in thermodynamic equilibrium at a given temperature and pressure is that their Gibbs free energies, $G(P, T)$, are equal. To determine T_m at any pressure, it is necessary to calculate G for the solid and liquid phases as a function of T and determine where they are equal. In fact, the Helmholtz free energy, $F(V, T)$, is generally calculated as a function of volume, V, and hence the pressure is obtained through the relation $P = -(\partial F/\partial V)_T$ and G through its definition, $G = F + PV$.

The ability of *ab initio* methods to provide accurate estimates of T_m was confirmed by studies on Al [156, 157], where it was possible to successfully reproduced the high

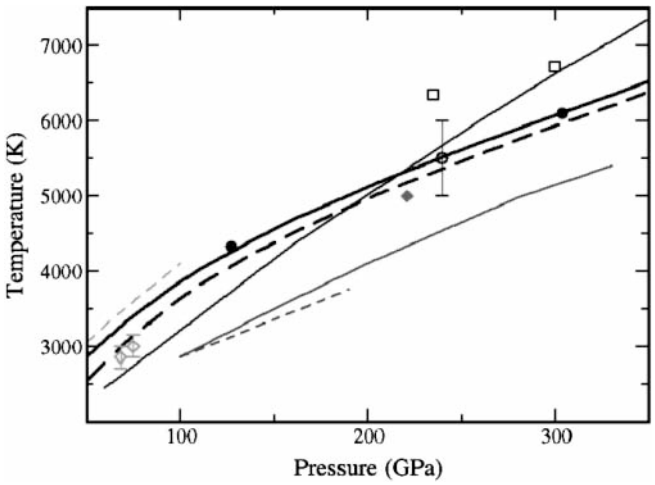

Fig 14. The calculated high P melting curve (solid black line) of Fe by Alfè et al. [148, 149] passes through the shock wave datum (open blue circle) [141]. Data shown includes: melting curve corrected for the GGA pressure error (black dashed line) [149], Belonoshko's melting curve (dark gray line) [150] and melting data corrected for errors in potential fitting (black dots), Laio et al. [151] melting curve (light gray line), Boehler's DAC curve (gray dashed line) [152], Shen's data (diamonds) [143], Yoo's shock data (open squares) [153], Williams's melting curve (pale gray dashed line) [154].

P melting behaviour of that element. Using a similar approach, Alfè et al. [148, 149] calculated T_m of Fe (as shown in Fig. 14), and they conclude that Fe melts at ICB pressures between 6200 and 6350 K. For pressures $P < 200$ GPa (the range covered by DAC experiments) the *ab initio* curve lies ~900 K above the experimental values of Boehler [152] and ~200 K above the more recent values of Shen et al. [143] (who stress that their values are only a lower bound to T_m). The *ab initio* curve falls significantly below the shock-based estimates for the T_m of Yoo et al. [153], in whose experiments temperature was deduced by measuring optical emission (however, the difficulties of obtaining temperature by this method in shock experiments are well known), but accords almost exactly with the shock data values [141, 144].

The composition and temperature of the core

The computational strategy recently used [135] for constraining the impurity fractions and the temperature of the core is based on the supposition that the solid inner core is slowly crystallising from the liquid outer core, and that therefore the inner and outer core are in thermodynamic equilibrium at the ICB. This implies that the chemical potentials of Fe and of each impurity must be equal on the two sides of the ICB. If the core consisted of pure Fe, equality of the chemical potential (Gibbs free energy in this case) would tell us only that the temperature at the ICB is equal to the melting temperature of Fe at the ICB pressure of 330 GPa. With impurities present, equality of the chemical potentials for each impurity element imposes a relation between the mole fractions in the liquid and the solid, so that if one simply considers S, O and Si, there are three such relations. But these three relations must be consistent with the accurate values of the mass densities in the inner and outer core deduced from seismic and free-oscillation data.

Alfè et al. [135] performed simulations at constant volume and temperature on systems of 64 atoms; the duration of the simulations after equilibration was typically 6 ps in order to reduce statistical errors to an acceptable level. Their results reveal a major qualitative difference between O and the other two impurities. For S and Si the chemical potential is almost the same in the solid and the liquid, the differences being at most 0.3 eV, i.e. markedly smaller than $k_BT \sim 0.5$ eV; but for O the difference of the chemical potential between solid and liquid is ~2.6 eV, which is much bigger than k_BT. This means that added O will partition strongly into the liquid, but added S or Si will have similar concentrations in the two phases.

Their simulations of the chemical potentials of the alloys can be combined with simulations of their densities to investigate whether the known densities of the liquid and solid core can be matched by any binary Fe/x system, with x = S, O or Si. Using their calculated partial volumes of S, Si and O in the binary liquid alloys, they find that the mole fractions required to reproduce the liquid core density are 16, 14 and 18% respectively (Fig. 15, panel (a) displays the predicted liquid density as a function of concentration, c_x, compared with the seismic density). Their calculated chemical potentials in the binary liquid and so-

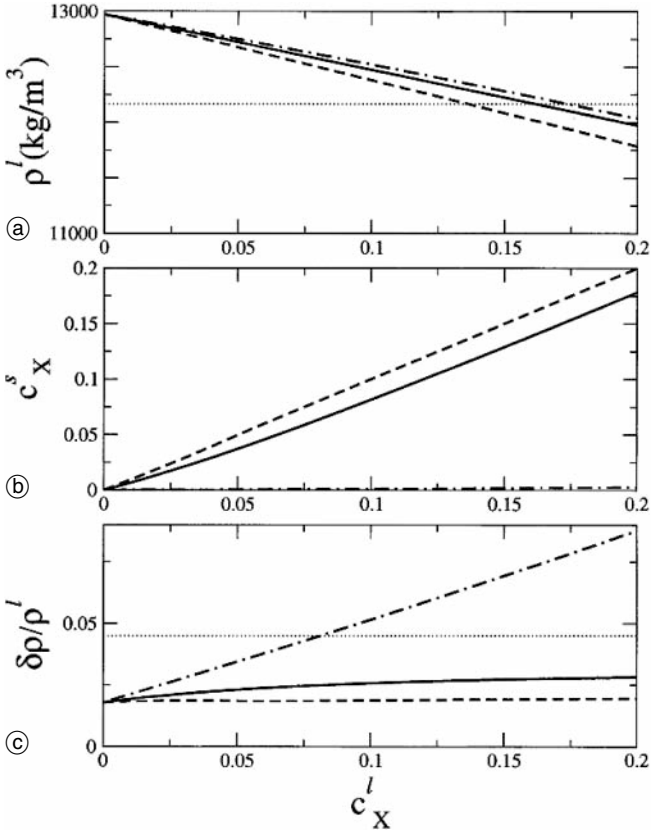

Fig. 15. Liquid and solid impurity mole fractions c_x^l and c_x^s of impurities $X = $ S, Si and O, and resulting densities of the inner and outer core predicted by *ab initio* simulations. Solid, dashed and chain curves represent S, Si and O respectively. (**a**) liquid density ϱ^l (kg m^{-3}); horizontal dotted line shows density from seismic data. (**b**) mole fractions in solid resulting from equality of chemical potentials in solid and liquid. (**c**) relative density discontinuity ($\delta\varrho/\varrho^l$) at the ICB; horizontal dotted line is the value from free oscillation data.

lid alloys then give the mole fractions in the solid of 14, 14 and 0.2% respectively that would be in equilibrium with these liquids (see Fig. 15, panel (b)). Finally, their partial volumes in the binary solids give ICB density discontinuities of 2.7 ± 0.5, 1.8 ± 0.5 and 7.8 ± 0.2% respectively (Fig. 15, panel (c)). As expected, for S and Si, the discontinuities are considerably smaller than the known value of 4.5 ± 0.5%; for O, the discontinuity is markedly greater than the known value. They conclude that none of the binary systems can account for the discontinuity quantitatively. However, it clearly can be accounted for by O together with either or both of S and Si. The estimated mole fractions needed to account for the ICB density discontinuity, were reported in [135] as being 8.5 ± 2.5 mole% S or Si and 0.2 ± 0.1% O in the inner core and 10 ± 2.5% S or Si and 8 ± 2.5% O in the liquid outer core. This compositional estimate was based on the value of the density discontinuity at the ICB determined by Shearer and Masters [158]. Since then, Masters and Gubbins [159] have reassessed the free oscillation data set, and have determined the density jump at the ICB to be 0.82 ± 0.18 Mg m^{-3}, which is larger than the previous estimates. Using the new density data [159] leads to a revised core composition of 7 ± 2.5 mole% S or Si and 0.2 ± 0.1% O for the inner core and 8 ± 2.5% S or Si and 13 ± 2.5% O for the outer core.

With the calculated impurity chemical potentials, the Gibbs-Duhem relation can be used to compute the liquidus temperature of the core alloy as being between 700 and 800 K lower than the melting temperature of pure Fe, and hence Alfè et al. [135] calculate that the Earth's temperature at the ICB to be between 5400 and 5650 K. Using this calculated value for the ICB temperature, and their *ab initio* values for the Grüneisen parameter, γ, for liquid Fe along the outer core adiabat [160] it is possible to determine the core temperature at the CMB, from the adiabatic temperature gradient, as being between 3950 and 4200 K.

Possible structure of the inner core

The conventional interpretation of the origin of the seismic anisotropy of the inner core is based on the idea of the development of partial alignment of the elastically anisotropic crystals of *hcp* Fe. The static elastic constant of *hcp* Fe were first calculated by Stixrude and Cohen [147]. The low temperature elastic constants of *hcp* Fe at 39 and 211 GPa were measured in an experiment reported by Mao et al. [161]. The overall agreement between the experimental and various *ab initio* studies is very good and calculated values compare well with experimental data at higher pressures, but discrepancies at lower pressures are probably due to the neglect of magnetic effects in the simulations.

The effect of temperature on the elastic constants of Fe was reported by Steinle-Neumann et al. [211] based on calculations using the approximate "particle in a cell" method. With increasing temperature, they found a significant change in the *c/a* axial ratio of the *hcp* structure, which in turn caused a marked reduction in the elastic constants c_{33}, c_{44} and c_{66}. This led them to conclude that increasing temperature reverses the sense of the single crystal longitudinal anisotropy of *hcp* Fe, and that the anisotropy of the core should now be viewed as being due to *hcp* Fe crystals having their *c*-axis preferably aligned equatorially, rather than axially as originally suggested [147]. However, the *ab initio* determination of high T elastic constants is very difficult. Recent calculations [211] have failed thus far to reproduce the strong effect of temperature on *c/a* reported in [211], and if this result is confirmed by more precise molecular dynamic simulations, then it will have important implications for the interpretation of the seismic tomography of the inner core.

The nature of inner core anisotropy has recently been shown to be more complex than previously thought, and Beghein and Trampert [163] have shown that free oscillation data cannot be simply interpreted in terms of the elastic properties of *hcp* Fe as reported in [211]. Furthermore, the assumption that *hcp* Fe is the thermodynamically stable polymorph of Fe at the high temperatures found in the inner core has also been recently questioned [140]. In spite of the arguments in favour of *hcp* Fe, it has been proposed by a number of workers that *bcc* Fe might be the stable high P/T phase [142, 164]. A strong argument in favour of the stability of *bcc* Fe under these conditions is that a number of transition metals (e.g. Ti, Zr) are known to transform from close-packed structures to the *bcc* structure at temperatures just below their melting

curve. However, until recently it appeared that theoretical calculations had ruled out the *bcc* structure as a candidate for the stable phase of Fe in the core. As reviewed in [137], this was because *ab initio* calculations have shown that the *bcc* structure becomes elastically unstable at pressures above ~150 GPa, and that the enthalpy of the perfect *bcc* structure is considerably higher than that of the *hcp* phase. However, these arguments are not conclusive because they are based on athermal or lattice dynamical *ab initio* calculations, which because of the dynamical instability of *bcc* Fe cannot be used to determine entropic effects at high pressures. In the past, computing limitations prevented a more sophisticated analysis, but recent methodological developments mean that it is now possible accurately to address these thermal effects.

Thus, to resolve the controversy over the effect of temperature on the stability of *bcc* Fe, Vočadlo et al. [160] recently performed *ab initio* molecular dynamics calculations on *bcc* Fe to simulate directly its behaviour at the high temperatures relevant to the Earth's inner core. They found that in all cases $F_{bcc} > F_{hcp}$, and so as previously concluded (on the basis of lattice dynamical as opposed to molecular dynamical calculations) pure Fe adopts the *hcp* structure at core pressures and temperatures. However, the differences in free energies are small (33–58 meV/atom along T_m). The Earth's inner core is known not to be made of pure Fe, but is expected to be alloyed with between 5 to 10 mol% of a lighter element. It is argued that, either separately or together, S and Si are two of the most probable light elements alloyed with Fe in the core. Recent experiments [165] have shown that at high pressures FeSi crystallises with the CsCl-structure (i.e. has identical atomic co-ordinates to *bcc*-Fe), and it has been found that at low concentrations Si favours the formation of *bcc* Fe over the *hcp* polymorph [166, 167]. Vočadlo et al. [160] therefore investigated the energetic effect of the substitution of S and Si in *bcc* and *hcp* Fe at representative core densities. They found that the enthalpies of the S and Si defects are respectively 1.4 and 1.2 eV per defect atom more stable in the *bcc* structure than in the *hcp* phase. Therefore, for example, a 5 mol% concentration of Si in Fe, would stabilise the *bcc* phase by 60 meV. Thus, they conclude that the presence of S or Si as the light impurity element in the core, at appropriate concentrations, could favour the formation of a *bcc*- rather than an *hcp*-structured Fe alloy phase at temperatures just below T_m at inner core pressure. The presence of a *bcc*-structured alloy may, therefore, be a candidate for explaining the observed seismic complexity of the inner core recently reported in [163], however more work on the high T elasticity of this and other candidate phases is needed before the seismic anisotropy of the inner core can be fully understood.

3. Giant planets

3.1 Jupiter and Saturn

Whether a planetary core exists in Jupiter and Saturn is not known for certain and its composition would be anyway unconstrained, so studies of the mineralogy of the giant planets have so far focused solely on the effects of pressure and temperature on hydrogen and on hydrogen/helium mixtures. Saturn emits more heat than it absorbs from the Sun. One of the possibile explanations for this anomalous luminosity is the energy released by gravitational differentiation of helium from hydrogen, with He gradually sinking towards the interior [168]. This is consistent with analyses of Voyager data that suggest a depletion of He from the Saturn's surface, with an atmospheric value of about 4–7.5% molar fraction (15–25% mass fraction, to be compared with an overall planetary value of 28%, as determined from the abundance of the primordial solar system) [13, 169]. The density profile of giant planets is poorly constrained (but the spacecraft Cassini is expected to refine the values of Saturn's gravitational moments J_4 and J_6, and thus to add better contraints on its density profile during this year's flyby). This poses important limitations not only to structural, but also to evolution models of giant planets, with implications for the history of the Solar System as a whole. Suggestions have been made that hydrogen could undergo a pressure-induced first-order transition, referred to as the plasma phase transition (PPT), possibly connected with molecular dissociation and/or metallization [170]. A first-order phase transition would have profound consequences on the planetary evolution and structure, if present [168]. First, it would generate an abrupt density and entropy jump at the transition pressure (depth). A density jump would affect primarily the internal modes, and might therefore be very difficult to detect. On the contrary, a jump in entropy would alter estimates of the central temperature by up to a factor of two. Moreover, a first-order phase transition in hydrogen would also affect strongly the partitioning of dissolved Helium, and would provide a likely reason for the helium rain-out described above. Finally, Jupiter and Saturn have magnetic fields, which is in the case of Jupiter is about 10 times stronger, at the surface, than the Earth magnetic field. The field is thought to originate from electrical currents generated by the pressure- and temperature-induced metallization of hydrogen.

Because the conditions found inside Jupiter and Saturn are more extreme than those found inside the Earth, computer simulations have been instrumental to shed light on some of the open issues highlighted above. We start our review of compressed hydrogen by describing how first-principle simulations have helped determining the high-pressure and high-temperature phase diagram of hydrogen, in more general terms. This is now known to consist of a low pressure phase I where molecules are centered on the sites of an *hcp* lattice, but are free to rotate around their center of mass, of an intermediate broken-symmetry phase II, where molecular rotations are hindered by the crystal field, of a high-pressure phase III, characterized by a strong infrared activity, and by one (or more) liquid phase(s) above melting. A large number of works have focused on the low-temperature portion of the phase diagram. Simulations on H_2 at low temperature are particularly challenging because of the need to include the possibility that the unit cell be large [171], combined with the very large number of points needed to sample the Brillouin zone [172]. This required the development of a new

method for Brillouin zone integration, based on perturbation theory [173]. Simulations in phase II have helped to understand its crystal structure, which on the basis of molecular dynamics within the GGA is either $Pca2_1$ or $P2_1c$ [174]. Simulations in phase III have suggested that the infrared activity might be due to a grouping of molecules in triplets [175]. More recently, it has been shown that most of the structures proposed so far are actually unstable mechanically, whereas structures with a layered triangular-like arrangement of molecules might be favored [176]. None of the above simulations has attempted to study the insulator-metal transition, expected to occur at sufficiently elevated pressures, because of intrinsic problems in the LDA (or GGA) approximation close to the metallic transition [177]. All the simulations described so far have assumed that the nuclei (protons) behave as classical particles, i.e. they obey Newton's equation. This approximation is not fully correct for hydrogen, where quantum effects are certainly important, e.g. in preserving rotational disorder in phase I down to very low temperatures. Path-integral MD simulations [178, 179] in phases I, II, and III have shown that the degree of order increases with pressure, and that quantum effects increase the localization of the protons, contrary to elementary considerations. However, at the temperatures of interest for planetary interiors quantum effects should play a negligible role, and have in fact been neglected in most DFT-based, but not in Quantum Monte Carlo (QMC) simulations. At finite temperature, first-principles simulations have been carried out to investigate the structure of the liquid at various conditions of pressure and temperature. At relatively low temperatures ($\sim$3000 K) and high pressures ($>$150 GPa) the liquid was found to be mostly monoatomic [180], although peculiar filamentary structures have been observed [181]. Recent *ab initio* simulations at pressure varying from 75 to 175 GPa and temperatures close to the freezing line (1500 K) have provided evidence for a liquid-liquid first-order transition between a molecular and a dissociated phase [182] (Fig. 16). The transition is accompanied by a 6% increase in density and by metallization. The transition might end at a critical point located below planetary temperatures and may not be directly related with the PPT described above. However, the nature of the liquid in the "supercritical" region above the critical point, that is along the pressure-temperature isentrope of giant planets, could be more complex than previously thought. A number of thermodynamic and dynamical anomalies are known to occur above the critical point. These include a maximum in the temperature dependence of the pressure along the isentrope [184] and a minimum in the pressure dependence of the sound velocity, with important implications for the interiors of giant planets [185].

The conductivity calculated with a Kubo-Greenwood formulation [180] appears to overestimate by almost one order of magnitude the conductivity measured along the multiple-shock compression curve achieved in gas-gun experiments [186]. Although this may indicate a problem in the determination of temperature in experiments, the discrepancy might also be attributed to the insufficient size of the simulation box. Determinations of the pressure-vs-density equation of state along the principal Hugoniot of deuterium [187, 188], i.e. at much higher temperatures and thus closer to the Jupitern and Saturn profiles, are in strong disagreement with laser-shock experiments [189], simulations showing a much smaller compressibility than experiments. Laser-shock experiments have been seriously questioned however. Inclusion of spin in the description of electronic states improves, but only marginally, the agreement [190]. At variance with the data at moderate temperatures ($\sim$3000 K), theoretical conductivities calculated [191] along the principal Hugoniot agree with optical reflectivity data [192]. Experimental and theoretical data for the conductivity of metallic compressed hydrogen are consistent with the strength and the complex pattern of the magnetic field measured at Jupiter [184]. Planetary models are however seriously challenged by atomistic simulations in at least two respects. The sound velocity of dense hydrogen calculated by first-principles molecular dynamics does not seem to be compatible with available planetary models [193]. Moreover, similar calculations have suggested that helium is fully miscible in hydrogen [194], again contrary to evidences from planetary modelling [195] but also with previous *ab initio* calculations [196]. More theoretical work is clearly needed before this issue can be considered as settled. Data from the Cassini spacecraft orbiting Saturn will be instrumental to provide further constraints on helium concentration and density profile.

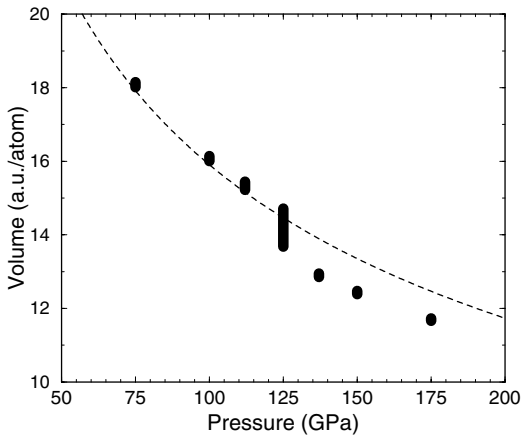

Fig. 16. Calculated volumes for liquid hydrogen at 1, 500 K (bars; their size gives the error). Calculations are based on *ab initio* molecular dynamics with supercells containing 448 hydrogen atoms [182]. A liquid-liquid phase transition is observed at 125 GPa. The dashed line indicates the experimental volume at 300 K [183].

3.2 Uranus and Neptune

Ab initio modelling of the planetary "ices" which compose Neptune and Uranus has so far focused primarily on trying to understand the properties of the three constituents – water, ammonia, and methane – separately.

The fate of methane (CH_4) at very high pressures and temperatures has received a lot of attention even before the Voyager flybys, in the early 80s, when shock-wave experiments have provided evidence of a transition that has been initially interpreted as due to full dissociation of methane into its consituent elements, carbon and hydrogen [197]. First-principles simulations have suggested that a more subtle chemistry may pre-empt full dissociation. For-

mation of hydrocarbons of molecular weight higher than methane has in fact been reported on the basis of constant-pressure simulations at 100 GPa and 4000 K [198]. Evidence for hydrocarbon formation has been later confirmed by static laser-heated diamond-anvil cell experiments [199], although at a considerably lower pressure than in the simulations. The separation of methane into rising hydrogen and sinking diamond likely releases gravitational energy to drive the convective motions of the planet's fluid interior. The amount of this energy appears to be large, comparable to the excess heat – over and above the heat received from the Sun – that infrared emissions indicate is released from Neptune's interior.

Water (H_2O) and ammonia (NH_3) appear at low pressure as molecular crystals or fluids held together by hydrogen bonds. Extreme conditions have the effect of changing the relative strength of the hydrogen bond, either by thermal induced partial breaking of the directional O–H...O linkage, or by its pressure-induced symmetrization. First-principles simulations have reproduced the pressure-induced symmetrization at low temperature [200, 201], although the precise value of the transition pressure could only be obtained by properly treating quantum effects on the protons [202]. The calculated infrared activity of ice across the symmetrization [203] compares favorably with experiments. At high temperature, partial collapse of the hydrogen bonding has been observed close to the critical point [204, 205], and its almost complete collapse has been reported at 10 GPa and 600 K [206]. At higher pressures and temperatures water becomes completely ionised, as a two-component fluid above melting and as a superionic phase below melting and for temperature above 2000 K [207]. Ionic conductivities in the fluid compare rather well with shock-wave measurements [208] at similar conditions. Experimental and theoretical conductivities are consistent with the strength of the magnetic field measured by Voyager during its flyby at Neptune and Uranus. Finally, water is predicted to become metallic at temperatures exceeding 7000 K and pressures above 300 GPa [207]. Whether or not metallic water contributes to the planetary magnetic field is not clear. Metallic water appears at conditions which are only realized close to the planetary core, so the total volume of the metallic component is probably small. Metallic conductivities are however at least one order of magnitude larger than ionic conductivities, so the overall contribution of metallic water to the magnetic field may not be negligible.

4. Conclusions

Over the last 10 years *ab initio* simulations have become a powerful tool for studies of matter, especially at extreme conditions where experimental information is limited. Since this tool is relatively new in planetary sciences, there are many open problems awaiting the application of such simulations. Among the most challenging problems are:

1. the elucidation of the chemical interaction between the Earth's core and mantle, including fractionation of Si, K, and siderophile elements
2. search for the structure of the phase III of hydrogen and the explanation of its infrared activity
3. more accurate studies of the miscibility in the H–He system and the fractionation of Ne between H and He
4. chemical reactions in the H_2O–NH_3–CH_4 system at planetary conditions, especially concerning diamond as a possible product.

Density functional theory (DFT) is the most popular (and usually the most accurate) basis for *ab initio* simulations. However, it has serious problems in describing van der Waals bonding and seriously underestimates band gaps in solids. Van der Waals forces become relatively less important than other contributions at high pressure – therefore, DFT is applicable even to molecular crystals at sufficiently high pressure [209]. The solution of the band gap problem is essential for the studies of metallisation under pressure. This problem is especially acute for Mott insulators, many of which (e.g., FeO) are represented as metals in standard DFT calculations – for more details on this problem see [210] and references therein. Mott insulators play a very special role in the Earth's mantle and core-mantle boundary, therefore further progress of computational methodology is needed for a wider application of first principles simulation techniques in Earth and planetary sciences.

Acknowledgments. ARO thanks CSCS (Manno) for access to supercomputers and ETH Zurich for funding.

References

[1] de Pater, I.; Lissauer, J. J.: Planetary Sciences. Cambridge University Press. Cambridge (2001) 529 pp.
[2] Dziewonski, A. M.; Anderson, D. L.: Preliminary Reference Earth Model. Phys. Earth Planet. Inter. **25** (1981) 297–356.
[3] Oganov, A. R.; Brodholt, J. P.; Price, G. D.: The elastic constants of $MgSiO_3$ perovskite at pressures and temperatures of the Earth's mantle. Nature **411** (2001) 934–937.
[4] Forte, A. M.; Mitrovica, J. X.: Deep-mantle high-viscosity flow and thermochemical structure inferred from seismic and geodynamic data. Nature **410** (2001) 1049–1056.
[5] Hemley, R. J.; Mao, H. K.: Overview of static high-pressure science. In Proc. of the International School of Physics: "*E. Fermi*" *on* "*High Pressure Phenomena*" (Eds. Hemley, R. J.; Chiarotti, G.; Bernasconi, M.; Ulivi, L.) Course CXLVII (IOS, Amsterdam) (2002) pp. 3–40.
[6] Anders, E.; Ebihara, M.: Solar system abundances of the elements. Geochim. Cosmochim. Acta **46** (1982) 2363–2380.
[7] Anderson, D. L.: Theory of the Earth. Blackwell Scientific Publications: Boston (1989) 366 pp.
[8] Ringwood, A. E.: Phase transformations and their bearing on the constitution and dynamics of the mantle. Geochim. Cosmochim. Acta **55** (1991) 2083–2110.
[9] Allègre, C. J.; Poirier, J.-P.; Humler, E.; Hofmann, A. W.: The chemical composition of the Earth. Earth Planet. Sci. Lett. **134** (1995) 515–526.
[10] Poirier, J.-P.: Introduction to the Physics of the Earth's Interior. 2nd edition. Cambridge University Press: Cambridge (2000) 326 pp.
[11] Bahcall, J. N.; Pinsonneault, M. H.: Solar models with helium and heavy-element diffusion. Rev. Mod. Phys. **67** (1995) 781–808.
[12] von Zahn, U.; Hunten, D. M.; Lehmacher, G.: Helium in Jupiter's atmosphere: Results from the Galileo probe Helium Interferometer Experiment. J. Geophys. Res. **103** (1998) 22815–22829.
[13] Conrath, B. J.; Gautier, D.: Saturn helium abundance: A reanalysis of Voyager measurements. Icarus **144** (2000) 124–134.
[14] Verhoogen, J.: Energetics of the Earth. National Academy Press: Washington (1980) 139 pp.

[15] Pearl, J. C.; Conrath, B. J.; Hanel, R. A.; Pirraglia, J. A.; Coustenis, A.: The albedo, effective temperature, and energy balance of Uranus, as determined from Voyager Iris data. Icarus **84** (1990) 12–28.
[16] Stanley, S.; Bloxham, J.: Convective-region geometry as the cause of Uranus' and Neptune's unusual magnetic fields. Nature **428** (2004) 151–153.
[17] Fiquet, G.: Mineral phases of the Earth's mantle. Z. Kristallogr. **216** (2001) 248–271.
[18] Oganov, A. R.; Ono, S.: Theoretical and experimental evidence for a post-perovskite phase of $MgSiO_3$ in Earth's D″ layer. Nature **430** (2004) 445–448.
[19] Murakami, M.; Hirose, K.; Kawamura, K.; Sata, N.; Ohishi, Y.: Post-perovskite phase transition in $MgSiO_3$. Science **304** (2004) 855–858.
[20] Duffy, T. H.; Hemley, R. J.; Mao, H. K.: Equation of state and shear strength at multimegabar pressures: magnesium oxide to 227 GPa. Phys. Rev. Lett. **74** (1995) 1371–1374.
[21] Mehl, M. J.; Cohen, R. E.; Krakauer, H.: Linearized augmented plane wave electronic structure calculations for MgO and CaO. J. Geophys. Res. **93** (1988) 8009–8022.
[22] Habas, M.-P.; Dovesi, R.; Lichanot, A.: The $B_1 \Leftrightarrow B_2$ phase transition in alkali-earth oxides: a comparison of *ab initio* Hartree-Fock and density functional calculations. J. Phys.: Condens. Matter **10** (1998) 6897–6909.
[23] Jaffe, J. E.; Snyder, J. A.; Lin, Z.; Hess, A. C.: LDA and GGA calculations for high-pressure phase transitions in ZnO and MgO. Phys. Rev. **B62** (2000) 1660–1665.
[24] Oganov, A. R.; Gillan, M. J.; Price, G. D.: *Ab initio* lattice dynamics and structural stability of MgO. J. Chem. Phys. **118** (2003) 10174–10182.
[25] Oganov, A. R.; Dorogokupets, P. I.: All-electron and pseudopotential study of MgO: Equation of state, anharmonicity, and stability. Phys. Rev. **B67** (2003) art. 224110.
[26] Speziale, S.; Zha, C.-S.; Duffy, T. S.; Hemley, R. J.; Mao, H.-K.: Quasi-hydrostatic compression of magnesium oxide to 52 GPa: Implications of the pressure-volume-temperature equation of state. J. Geophys. Res. **B106** (2001) 515–528.
[27] Robie, R. A.; Hemingway, B. S.: Thermodynamic Properties of Minerals and Related Substances at 289.15 K and 1 bar (10^5 Pascals) Pressure and at Higher Temperatures, U.S. Geological Survey Bulletin, Washington (1995) 2131.
[28] Karki, B. B.; Stixrude, L.; Clark, S. J.; Warren, M. C.; Ackland, G. J.; Crain, J.: Structure and elasticity of MgO at high pressure. Am. Mineral. **82** (1997) 51–60.
[29] Sinogeikin, S. V.; Bass, J. D.: Single-crystal elasticity of pyrope and MgO to 20 GPa by Brillouin scattering in the diamond cell. Phys. Earth Planet. Inter. **120** (2000) 43–62.
[30] Zha, C.-S.; Mao, H.-K.; Hemley, R. J.: Elasticity of MgO and a primary pressure scale to 55 GPa. Proc. Natl. Acad. Sci. USA **97** (2000) 13494–13499.
[31] Merkel, S.; Wenk, H. R.; Shu, J. F.; Shen, G. Y.; Gillet, P.; Mao, H. K.; Hemley, R. J.: Deformation of polycrystalline MgO at pressures of the lower mantle. J. Geophys. Res. **107** (2002) art. 2271.
[32] Drummond, N. D.; Ackland, G. J.: *Ab initio* quasiharmonic equations of state for dynamically stabilized soft-mode materials. Phys. Rev. **B65** (2002) art. 184104.
[33] Strachan, A.; Çağin, T.; Goddard, W. A.: III Phase diagram of MgO from density-functional theory and molecular-dynamics simulations. Phys. Rev. **B60** (1999) 15084–15093.
[34] Baroni, S.; de Gironcoli, S.; Dal Corso, A.; Gianozzi, P.: Phonons and related crystal properties from density-functional perturbation theory. Rev. Mod. Phys. **73** (2001) 515–562.
[35] Gonze, X.; Rignanese, G.-M.; Caracas, R.: First-principle studies of the lattice dynamics of crystals, and related properties. Z. Kristallogr. **220** (2005) 458–472.
[36] Badro, J.; Struzhkin, V. V.; Shu, J.; Hemley, R. J.; Mao, H.-K.; Kao, C.-C.; Rueff, J.-P.; Shen, G.: Magnetism in FeO at megabar pressures from X-ray emission spectroscopy. Phys. Rev. Lett. **83** (1999) 4101–4104.
[37] Dubrovinsky, L. S.; Dubrovinskaia, N. A.; Saxena, S. K.; Annersten, H.; Halenius, E.; Harryson, H.; Tutti, F.; Rekhi, S.; Le Bihan, T.: Stability of ferropericlase in the lower mantle. Science **289** (2000) 430–432.
[38] Lin, J. F.; Heinz, D. L.; Mao, H. K.; Hemley, R. J.; Devine, J. M.; Li, J.; Shen, G. Y.: Stability of magnesiowustite in Earth's lower mantle. Proc. Natl. Acad. Sci. USA **100** (2003) 4405–4408.
[39] Kingma, K. J.; Cohen, R. E.; Hemley, R. J.; Mao, H.-K.: Transformations of stishovite to a denser phase at lower-mantle pressures. Nature **374** (1995) 243–245.
[40] Lee, C.; Gonze, X.: The pressure-induced ferroelastic phase transition of SiO_2 stishovite. J. Phys. : Condens. Matter **7** (1995) 3693–3698.
[41] Dubrovinsky, L. S.; Saxena, S. K.; Lazor, P.; Ahuja, R.; Eriksson, O.; Wills, J. M.; Johansson, B.: Experimental and theoretical identification of a new high-pressure phase of silica. Nature **388** (1997) 362–365.
[42] Karki, B. B.; Warren, M. C.; Stixrude, L.; Ackland, G. J.; Crain, J.: *Ab initio* studies of high-pressure structural transformations in silica. Phys. Rev. **B55** (1997) 3465–3471. (Erratum: Phys. Rev. **B56**, 2884).
[43] Teter, D. M.; Hemley, R. J.; Kresse, G.; Hafner, J.: High pressure polymorphism in silica. Phys. Rev. Lett. **80** (1998) 2145–2148.
[44] Ono, S.; Hirose, K.; Murakami, M.; Isshiki, M.: Post-stishovite phase boundary in SiO_2 determined by in situ X-ray observations. Earth Planet. Sci Lett. **197** (2002) 198–192.
[45] Shieh, S. R.; Duffy, T. S.; Li, B.: Strength and elasticity of SiO_2 across the stishovite-$CaCl_2$-type structural phase boundary. Phys. Rev. Lett. **89** (2002) art. 255507.
[46] Akins, J. A.; Ahrens, T. J.: Dynamic compression of SiO_2: a new interpretation. Geophys. Res. Lett. **29** (2002) art. 10.1029/2002GL014806.
[47] Murakami, M.; Hirose, K.; Ono, S.; Ohishi, Y.: Stability of $CaCl_2$-type and alpha-PbO_2-type SiO_2 at high pressure and temperature determined by in-situ X-ray measurements. Geophys. Res. Lett. **30** (2003) art. 1207.
[48] Andrault, D.; Fiquet, G.; Guyot, F.; Hanfland, M.: Pressure-induced Landau-type transition in stishovite. Science **282** (1998) 720–724.
[49] Oganov, A. R.; Gillan, M. J.; Price, G. D.: Structural stability of silica at high pressures and temperatures. Phys. Rev. B**71** (2005) art. 064104.
[50] Dubrovinskaia, N. A.; Dubrovinsky, L. S.; Saxena, S. K.; Tutti, F.; Rekhi, S.; Le Bihan, T.: Direct transition from cristobalite to post-stishovite α-PbO_2-like silica phase. Eur. J. Mineral. **13** (2001) 479–483.
[51] Dubrovinsky, L. S.; Dubrovinskaya, N. A.; Saxena, S. K.; Tutti, F.; Rekhi, S.; Le Bihan, T.; Shen, G.; Hu, J.: Pressure-induced transformations of cristobalite. Chem. Phys. Lett. **333** (2001) 264–270.
[52] Haines, J.; Leger, J. M.; Schulte, O.: $Pa\bar{3}$ modified fluorite-type structures in metal dioxides at high pressure. Science **271** (1996) 629–631.
[53] Ono, S.; Tsuchiya, T.; Hirose, K.; Ohishi, Y.: High-pressure form of pyrite-type germanium oxide. Phys. Rev. B**68** (2003) art. 014103.
[54] Bader, R. F. W.: Atoms in Molecules. A Quantum Theory. Oxford University Press, Oxford (1990).
[55] Kirfel, A.; Krane, H.-G.; Blaha, P.; Schwarz, K.; Lippmann, T.: Electron-density distribution in stishovite, SiO_2: a new high-energy synchrotron-radiation study. Acta Cryst. **A57** (2001) 663–677.
[56] Marton, F. C.; Cohen, R. E.: Prediction of a high-pressure phase transition in Al_2O_3. Am. Mineral. **79** (1994) 789–792.
[57] Duan, W.; Wentzcovitch, R. M.; Thomson, K. T.: First-principles study of high-pressure alumina polymorphs. Phys. Rev. **B57** (1998) 10363–10369.
[58] Oganov, A. R.; Ono, S.: New high-pressure phase of alumina (Al_2O_3). (2005) submitted.
[59] Funamori, N.; Jeanloz, R.: High-pressure transformation of Al_2O_3. Science **278** (1997) 1109–1111.
[60] Lin, J.-F.; Degtyareva, O.; Prewitt, C. T.; Dera, P.; Sata, N.; Gregoryanz, E.; Mao, H.-K.; Hemley, R. J.: Crystal structure

of a high-pressure/high-temperature phase of alumina by *in situ* X-ray diffraction. Nature Materials **3** (2004) 389–393.
[61] Ahmed-Zaid, I.; Madon, M.: A high-pressure form of Al_2SiO_5 as a possible host of aluminium in the lower mantle. Nature **353** (1991) 426–428.
[62] Schmidt, M. W.; Poli, S.; Comodi, P.; Zanazzi, P. F.: High-pressure behavior of kyanite: Decomposition of kyanite into stishovite and corundum. Am. Mineral. **82** (1997) 460–466.
[63] Oganov, A. R.; Brodholt, J. P.: High-pressure phases in the Al_2SiO_5 system and the problem of Al-phase in Earth's lower mantle: *ab initio* pseudopotential calculations. Phys. Chem. Minerals **27** (2000) 430–439.
[64] Wood, B. J.; Rubie, D. C.: The effect of alumina on the phase transformations at the 660-kilometer discontinuity from Fe–Mg partitioning experiments. Science **273** (1996) 1522–1524.
[65] McCammon, C.: Perovskite as a possible sink for ferric iron in the lower mantle. Nature **387** (1997) 694–696.
[66] Frost, D. J.; Langenhorst, F.: The effect of Al_2O_3 on Fe–Mg partitioning between magnesiowustite and magnesium silicate perovskite. Earth Planet. Sci. Lett. **199** (2002) 227–241.
[67] Zhang, J. Z.; Weidner, D. J.: Thermal equation of state of aluminum-enriched silicate perovskite. Science **284** (1999) 782–784.
[68] Andrault, D.; Bolfan-Casanova, N.; Guignot, N.: Equation of state of lower mantle (Al,Fe)–$MgSiO_3$ perovskite. Earth Planet. Sci. Lett. **193** (2001) 501–508.
[69] Brodholt, J. P.: Pressure-induced changes in the compression mechanism of aluminous perovskite in the Earth's mantle. Nature **407** (2000) 620–622.
[70] Yamamoto, T.; Yuen, D. A.; Ebisuzaki, T.: Substitution mechanism of Al ions in $MgSiO_3$ perovskite under high pressure conditions from first-principles calculations. Earth Planet. Sci. Lett. **206** (2003) 617–625.
[71] Irifune, T.: Absence of an aluminous phase in the upper part of the Earth's lower mantle. Nature **370** (1994) 131–133.
[72] Irifune, T.; Fujino, K.; Ohtani E.: A new high-pressure form of $MgAl_2O_4$. Nature **349** (1991) 409–411.
[73] Funamori, N.; Jeanloz, R.; Nguyen, J.; Kavner, A.; Caldwell, W. A.; Fujino, K.; Miyajima, N.; Shinmei, T.; Tomioka, N.: High-pressure transformations in $MgAl_2O_4$. J. Geoph. Res. **103** (1998) 20813–20818.
[74] Madon, M.; Castex, J.; Peyronneau, J.: A new aluminocalcic high-pressure phase as a possible host of calcium and aluminium in the lower mantle. Nature **342** (1989) 422–424.
[75] Oganov, A. R.; Price, G. D.; Brodholt, J. P.: Theoretical investigation of metastable Al_2SiO_5 polymorphs. Acta Cryst. **A57** (2001) 548–557.
[76] Sherman, D. M.: The high-pressure electronic structure of magnesiowüstite (Mg,Fe)O – applications to the physics and chemistry of the lower mantle. J. Geophys. Res. **96** (1991) 14299–14312.
[77] Isaak, D. G.; Cohen, R. E.; Mehl, M. J.; Singh, D. J.: Phase stability of wüstite at high pressure from first-principles linearized augmented plane-wave calculations. Phys. Rev. **B47** (1993) 7720–7731.
[78] Cohen, R. E.; Mazin, I. I.; Isaak, D. G.: Magnetic collapse in transition metal oxides at high pressure: implications for the Earth. Science **275** (1997) 654–657.
[79] Cohen, R. E.: Bonding and electronic structure of minerals. In: *Miscroscopic Properties and Processes in Minerals*. NATO Science Series, v. C543. (Eds. Wright, K.; Catlow, R.), Kluwer: Dordrecht, (1999) pp. 201–264.
[80] Fang, Z.; Solovyev, I. V.; Sawada, H.; Terakura, K.: First-principles study on electronic structures and phase stability of MnO and FeO under high pressure. Phys. Rev. **B59** (1999) 762–774.
[81] Gramsch, S. A.; Cohen, R. E.; Savrasov, S. Y.: Structure, metal-insulator transitions, and magnetic properties of FeO at high pressures. Am. Mineral. **88** (2003) 257–261.
[82] Pasternak, M. P.; Taylor, R. D.; Jeanloz, R.; Li, X.; Nguyen, J. H.; McCammon, C. A.: High pressure collapse of magnetism in $Fe_{0.94}O$: Mossbauer spectroscopy beyond 100 GPa. Phys. Rev. Lett. **79** (1997) 5046–5049.
[83] Badro, J.; Struchkin, V. V.; Shu, J. F.; Hemley, R. J.; Mao, H. K.; Kao, C. C.; Rueff, J. P. Shen, G. Y.: Magnetism in FeO at megabar pressures from X-ray emission spectroscopy. Phys. Rev. Lett. **83** (1999) 4101–4104.
[84] Liechtenstein, A. I.; Anisimov, V. I.; Zaanen, J.: Density functional theory and strong interactions – orbital ordering in Mott-Hubbard insulators. Phys. Rev. **B52** (1995) R5467–R5470.
[85] Dudarev, S. L.; Botton, G. A.; Savrasov, S. Y.; Szotek, Z.; Temmerman, W. M.; Sutton, A. P.: Electronic structure and elastic properties of strongly correlated metal oxides from first principles: LSDA + U, SIC-LSDA and EELS study of UO_2 and NiO. Phys. Stat. Sol. **166** (1998) 429–443.
[86] Willis, B. T. M.; Rooksby, H. P.: Change of structure of ferrous oxide at low temperature. Acta Cryst. **6** (1953) 827–831.
[87] Roth, W. L.: Magnetic structures of MnO, FeO, CoO, and NiO. Phys. Rev. **110** (1958) 1333–1341.
[88] Shim, S. H.; Jeanloz, R.; Duffy, T. S.: Tetragonal structure of $CaSiO_3$ perovskite above 20 GPa. Geophys. Res. Lett. **29** (2002) 2166.
[89] Ono, S.; Ohishi, Y.; Mibe, K.: Phase transition of Ca-perovskite and stability of Al-bearing Mg-perovskite in the lower mantle. Am. Mineral. **89** (2004) 1480–1485.
[90] Wentzcovitch, R.; Ross, N. L.; Price, G. D.: *Ab initio* study of $MgSiO_3$ and $CaSiO_3$ perovskites at lower-mantle pressures. Phys. Earth Planet. Int. **90** (1995) 101–112.
[91] Warren, M. C.; Ackland, G. J.; Karki, B. B.; Clark, S. J.: Phase transitions in silicate perovskites from first principles. Miner. Mag. **62** (1998) 585–598.
[92] Chizmeshya, A. V. G.; Wolf, G. H.; McMillan, P. F.: First-principles calculation of the equation-of-state, stability, and polar optic modes of $CaSiO_3$ perovskite. Geophys. Res. Lett. **23** (1996) 2725–2728. (correction in: *ibid.* (1998) **25**, 711).
[93] Stixrude, L.; Cohen, R. E.; Yu, R. C.; Krakauer, H.: Prediction of phase transition in $CaSiO_3$ perovskite and implications for lower mantle structure. Am. Mineral. **81** (1996) 1293–1296.
[94] Magyari-Köpe, B.; Vitos, L.; Grimavall, G.; Johansson, B.; Kollar, J.: Low-temperature crystal structure of $CaSiO_3$ perovskite: An *ab initio* total energy study. Phys. Rev. **B65** (2002) art. 193107.
[95] Akber-Knutson, S.; Bukowinski, M. S. T.; Matas, J.: On the structure and compressibility of $CaSiO_3$ perovskite. Geophys. Res. Lett. **29** (2002) 1034–1037.
[96] Kresse, G.; Joubert, D.: From ultrasoft pseudopotentials to the projector augmented-wave method. Phys. Rev. **B59** (1999) 1758–1775.
[97] Holzwarth, N. A. W.; Matthews, G. E.; Dunning, R. B.; Tackett, A. R.; Zeng, Y.: Comparison of the projector augmented-wave, pseudopotential, and linearized augmented-plane-wave formalisms for density-functional calculations of solids. Phys. Rev. **B55** (1997) 2005–2017.
[98] Vinnik, L.; Kato, M.; Kawakatsu, H.: Search for seismic discontinuities in the lower mantle. Geophys. J. Int. **147** (2001) 41–56.
[99] D'Arco, Ph.; Sandrone, G.; Dovesi, R.; Orlando, R.; Saunders, V. R.: A quantum mechanical study of the perovskite structure type of $MgSiO_3$. Phys. Chem. Minerals **20** (1993) 407–414.
[100] D'Arco, Ph.; Sandrone, G.; Dovesi, R.; Apra, E.; Saunders, V. R.: A quantum-mechanical study of the relative stability under pressure of $MgSiO_3$-ilmenite, $MgSiO_3$-perovskite, and MgO-periclase + SiO_2-stishovite assemblage. Phys. Chem. Minerals **21** (1994) 285–293.
[101] Wentzcovitch, R. M.; Martins, J. L.; Price, G. D.: *Ab initio* molecular dynamics with variable cell shape: application to $MgSiO_3$. Phys. Rev. Lett. **70** (1993) 3947–3950.
[102] Stixrude, L.; Cohen, R. E.: Stability of orthorhombic $MgSiO_3$ perovskite in the Earth's lower mantle. Nature **364** (1993) 613–616.
[103] Warren, M. C.; Ackland, G. J.: *Ab initio* studies of structural instabilities in magnesium silicate perovskite. Phys. Chem. Minerals **23** (1996) 107–118.
[104] Oganov, A. R.; Brodholt, J. P.; Price; G. D.: *Ab initio* elasticity and thermal equation of state of $MgSiO_3$ perovskite. Earth Planet. Sci. Lett. **184** (2001) 555–560.

[105] O'Keeffe, M.; Bovin, J. O.: Solid electrolyte behavior of $NaMgF_3$: geophysical implications. Science **206** (1979) 599–600.
[106] Matsui, M.; Price, G. D.: Simulation of the pre-melting behaviour of $MgSiO_3$ perovskite at high pressures and temperatures. Nature **351** (1991) 735–737.
[107] Serghiou, G.; Zerr, A.; Boehler, R.: $(Mg,Fe)SiO_3$-perovskite stability under lower mantle conditions. Science **280** (1998) 2093–2095.
[108] Shim, S. H.; Duffy, T. S.; Shen, G. Y.: Stability and structure of $MgSiO_3$ perovskite to 2300-kilometer depth in Earth's mantle. Science **293** (2001) 2437–2440.
[109] Luo, S. N.; Mosenfelder, J. L.; Asimow, P. D.; Ahrens, T. J.: Direct shock wave loading of Stishovite to 235 GPa: Implications for perovskite stability relative to an oxide assemblage at lower mantle conditions. Geophys. Res. Lett. **29** (2002) art. 1691.
[110] Saxena, S. K.; Dubrovinsky, L. S.; Lazor, P.; Cerenius, Y.; Häggkvist, P.; Hanfland, M.; Hu, J.: Stability of perovskite ($MgSiO_3$) in the Earth's mantle. Science **274** (1996) 1357–1359.
[111] Oganov, A. R.; Price, G. D.: Ab initio thermodynamics of $MgSiO_3$ perovskite at high pressures and termperatures. J. Chem. Phys. **122** (2005) art. 124501.
[112] Karki, B. B.; Stixrude, L.; Clark, S. J.; Warren, M. C.; Ackland, G. J.; Crain, J.: Elastic properties of orthorhombic $MgSiO_3$ perovskite at lower mantle pressures. Am. Mineral. **82** (1997) 635–638.
[113] Wentzcovitch, R. M.; Karki, B. B.; Karato, S.; da Silva, C. R. S.: High pressure elastic anisotropy of $MgSiO_3$ perovskite and geophysical implications. Earth Planet. Sci. Lett. **164** (1998) 371–378.
[114] Marton, F. C.; Cohen, R. E.: Constraints on lower mantle composition from molecular dynamics simulations of $MgSiO_3$ perovskite. Phys. Earth Planet. Int. **134** (2002) 239–252.
[115] Wentzcovitch, R. M.; Karki, B. B.; Cococcioni, M.; de Gironcoli, S.: Thermoelastic properties of $MgSiO_3$ perovskite: Insights on the nature of the Earth's lower mantle. Phys. Rev. Lett. **92** (2004) art. 018501.
[116] Yeganeh-Haeri, A.: Synthesis and re-investigation of the elastic properties of single-crystal magnesium silicate perovskite. Phys. Earth Planet. Inter. **87** (1994) 111–121.
[117] Sinelnikov, Y. D.; Chen, G.; Neuville, D. R.; Vaughan, M. T.; Liebermann, R. C.: Ultrasonic shear wave velocities of $MgSiO_3$ perovskite at 8 GPa and 800 K and lower mantle composition. Science **281** (1998) 677–679.
[118] Oganov, A. R.; Brodholt, J. P.; Price, G. D.: *Ab initio* theory of thermoelasticity and phase transitions in minerals, in C. M. Gramaccioli (ed.), Energy Modelling in Minerals, EMU Notes in Mineralogy, v.4, Eötvös University Press, Budapest, (2002) pp. 83–170.
[119] Brown, J. M.; Shankland, T. J.: Thermodynamic properties in the Earth as determined from seismic profiles. Geophys. J. R. Astr. Soc. **66** (1981) 579–596.
[120] Anderson, O. L.: The Earth's core and the phase diagram of iron. Phil. Trans. R. Soc. Lond. A**306** (1982) 21–35.
[121] Ito, E.; Katsura, T.: A temperature profile of the mantle transition zone. Geophys. Res. Lett. **16** (1989) 425–428.
[122] Ono, S.; Oganov, A. R.; Ohishi, Y.: *In situ* observations of phase transition between perovskite and $CaIrO_3$-type phase in $MgSiO_3$ and pyrolitic mantle composition. (2004) submitted.
[123] Alfè, D.; Gillan, M. J.; Price, G. D.: Composition and temperature of the Earth's core constrained by combining *ab initio* calculations and seismic data. Earth Planet. Sci. Lett. **195** (2002) 91–98.
[124] Zerr, A.; Diegler, A.; Boehler, R.: Solidus of Earth's deep mantle. Science **281** (1998) 243–246.
[125] Williams, Q.; Garnero, E.: Seismic evidence for partial melt at the base of Earth's mantle. Science **273** (1996) 1528–1530.
[126] Sidorin, I.; Gurnis, M.; Helmberger, D. V.: Evidence for a ubiquitous seismic discontinuity at the base of the mantle. Science **286** (1999) 1326–1331.
[127] Ono, S.; Kikegawa, T.; Ohishi, Y.: High-pressure phase transition of hematite, Fe_2O_3. J. Phys. Chem. Solid **65** (2004) 1527–1530.
[128] Zharkov, V. N.; Kalinin, V. A.: Equations of state of solids at high pressures and temperatures. Consult. Bur.: New York (1971).
[129] Bukowinski, M. S. T.: Quantum geophysics. Ann. Rev. Earth Planet. Sci. **22** (1994) 167–205.
[130] Birch, F.: Elasticity and the constitution of the Earth's interior. J. Geophys. Res. **57** (1952) 227–286.
[131] Poirier, J. P.: Light elements in the Earth's outer core: A critical review. Phys. Earth Planet. Inter. **85** (1994a) 319–337.
[132] Poirier, J. P.: Physical-properties of the Earths core. Cr. Acad. Sci. II. **318** (1994b) 341–350.
[133] Allègre, C. J.; Poirier, J. P.; Humler, E.; Hofmann, A. W.: The chemical composition of the Earth. Phys. Earth Planet. Interiors. **134** (1995) 515–526.
[134] McDonough, W. F.; Sun, S.-S.: The composition of the Earth. Chem. Geol. **120** (1995) 223–253.
[135] Alfè, D.; Gillan, M. J.; Price, G. D.: Composition and temperature of the Earth's core constrained by combining *ab initio* calculations and seismic data. Earth Planet. Sci. Lett. **195** (2002) 91–98.
[136] Stixrude, L.; Brown, J. M.: The Earth's Core. In: *Ultrahigh-pressure Mineralogy* (ed. R. J. Hemley). Reviews in Mineralogy **37** (1998) 261–283.
[137] Steinle-Neumann, G.; Stixrude, L.; Cohen, R. E.: Physical properties of iron in the inner core. In: *Earth's Core* (eds. V. Dehant, K. C. Creager, S.-I. Karato, S. Zatman). AGU, Geodynamics Series **31** (2003) 137–162.
[138] Saxena, S. K.; Dubrovinsky, L. S.; Häggkvist, P.: X-ray evidence for the new phase of β-iron at high temperature and high pressure. Geophys. Res. Lett. **23** (1996) 2441–2444.
[139] Andrault, D.; Fiquet, G.; Kunz, M.; Visocekas, F.; Häusermann, D.: The orthorhombic structure of iron: an in situ study at high temperature and high pressure. Science. **278** (1997) 831–834.
[140] Brown, J. M.: The equation of state of Iron to 450 GPa: another high pressure solid phase? Geophys. Res. Letts. **28** (2001) 4339–4342.
[141] Brown, J. M.; McQueen, R. G.: Phase transitions, Grüneisen parameter and elasticity for shocked iron between 77 GPa and 400 GPa. J. Geophys. Res. **91** (1986) 7485–7494.
[142] Matsui, M.; Anderson, O. L.: The case for a body-centered cubic phase for iron at inner core conditions. Physics Earth Planetary Interiors. **103** (1997) 55–62.
[143] Shen, G. Y.; Mao, H. K.; Hemley, R. J.; Duffy, T. S.; Rivers, M. L.: Melting and crystal structure of iron at high pressures and temperatures. Geophys. Res. Lett. **25** (1998) 373.
[144] Nguyen, J. H.; Holmes, N. C.: Iron sound velocities in shock wave experiments. Shock Compression of Condensed Matter. **CP505** (1999) 81–84.
[145] Vočadlo, L.; Brodholt, J.; Alfè, D.; Price, G. D.; Gillan, M. J.: The structure of iron under the conditions of the Earth's inner core. Geophys. Res. Lett. **26** (1999) 1231–1234.
[146] Söderlind, P.; Moriarty, J. A.; Wills, J. M.: First-principles theory of iron up to earth-core pressures: Structural, vibrational and elastic properties. Phys. Rev. **B53** (1996) 14063–14072.
[147] Stixrude, L.; Cohen, R. E.: Constraints on the Crystalline Structure of the Inner Core Mechanical Instability of *bcc* Iron at High-Pressure. Geophys. Res. Lett. **22** (1995) 125–128.
[148] Alfè, D.; Gillan, M. J.; Price, G. D.: The melting curve of iron at the pressures of the Earth's core from *ab initio* calculations. Nature **401** (1999) 462–464.
[149] Alfè, D.; Price, G. D.; Gillan, M. J.: Iron under Earth's core conditions: Liquid-state thermodynamics and high-pressure melting curve from *ab initio* calculations. Phys. Rev. **B65** (2002) 165118.
[150] Belonoshko, A. B.; Ahuja, R.; Johansson, B.: Quasi-*ab initio* molecular dynamic study of Fe melting. Phys. Rev. Lett. **84** (2000) 3638–3641.
[151] Laio, A.; Bernard, S.; Chiarotti, G. L.; Scandolo, S.; Tosatti, E.: Physics of iron at Earth's core conditions. Science **287** (2000) 1027–1030.
[152] Boehler, R.: Temperature in the Earth's core from the melting point measurements of iron at high static pressures. Nature **363** (1993) 534–536.

[153] Yoo, C. S.; Holmes, N. C.; Ross, M.; Webb, D. J.; Pike, C.: Shock temperatures and melting of iron at Earth core conditions. Phys. Rev. Lett. **70** (1993) 3931–3934.
[154] Williams, Q.; Jeanloz, R.; Bass, J.; Svendsen, B.; Ahrens, T. J.: The melting curve of iron to 250 GPa: a constraint on the temperature at the the Earth's centre. Science **236** (1987) 181–182.
[155] Shen, G. Y.; Heinze, D. L.: High Pressure melting of deep mantle and core materials. In: *Ultrahigh-pressure Mineralogy* (ed. R. J. Hemley). Reviews in Mineralogy **37** (1998) 369–398.
[156] de Wijs, G. A.; Kresse, G.; Gillan, M. J.: First order phase transitions by first principles free energy calculations: The melting of Al. Phys. Rev. **B57** (1998) 8233–8234.
[157] Vočadlo, L.; Alfè, D.: The *ab initio* melting curve of aluminum. Phys. Rev. **B65** (2002) 214105.
[158] Shearer, P. M.; Masters, G.: The density and shear velocity contrast at the inner core boundary. Geophys. J. Int. **102** (1990) 491–498.
[159] Masters, G.; Gubbins, D.: On the resolution of density within the Earth. Phys. Earth Planet. In. **140** (2003) 159–167.
[160] Vočadlo, L.; Alfè, D.; Gillan, M. J.; Wood, I. G.; Brodholt, P. J.; Price, G. D.: Possible thermal and chemical stabilisation of body-centred-cubic iron in the Earth's core? Nature **424** (2003) 536–539.
[161] Mao, H. K.; Shu, J.; Shen, G.; Hemley, R. J.; Li, B.; Singh, A. K.: Elasticity and rheology of iron above 220 GPa and the nature of the Earth's inner core. Nature **399** (1999) 280.
[162] Gannarelli, C. M. S.; Alfè, D.; Gillan, M. J.: The particle-in-cell model for *ab initio* thermodynamics: implications for the elastic anisotropy of the Earth's inner core. Physics of the Earth and Planetary Interiors **139** (2003) 243–253.
[163] Beghein, C.; Trampert, J.: Robust Normal Mode Constraints on Inner-Core Anisotropy from Model Space Search. Science **299** (2003) 552–555.
[164] Ross, M.; Young, D. A.; Grover, R.: Theory of the iron phase diagram at Earth core conditions. J. Geophys. Res. **95** (1990) 21713–21716.
[165] Dobson, D. P.; Vočadlo, L.; Wood, I. G.: A new high-pressure phase of FeSi. Amer. Mineral. **87** (2002) 784–787.
[166] Lin, J.-F.; Heinz, D. L.; Campbell, A. J.; Devine, J. M.; Shen, G.: Iron-silicon alloy in Earth's core? Science **295** (2002) 313–315.
[167] Dubrovinsky, L.; Dubrovinskaia, N.; Langenhorst, F.; Dobson, D.; Rubie, D.; Gessmann, C.; Abrikosov, I. A.; Johansson, B.; Baykov, V. I.; Vitos, L.; Le Bihan, T.; Crichton, W. A.; Dmitriev, V.; Weber, H. P.: Iron-silica interaction at extreme conditions and the electrically conducting layer at the base of Earth's mantle. Nature **422** (2003) 58–61.
[168] Stevenson, D. J.: States of matter in massive planets. J. Phys.: Cond. Matter **10** (1998) 11227–11234.
[169] Conrath, B. J.; Gautier, D.; Hanel, R. A.; Hornstein, J. S.: The helium abundance of Saturn from Voyager measurements, Astrophys. J. **282** (1984) 807–815.
[170] Chabrier, G.; Saumon, D.; Hubbard, W. B.; Lunine, J. I.: The molecular-metallic transition of hydrogen and the structure of Jupiter and Saturn. Astrophys. J. **391** (1992) 817–826.
[171] Goncharov, A. F.; Hemley, R. J.; Mao, H.-K.; Shu, J. F.: New high-pressure excitations in parahydrogen. Phys. Rev. Lett. **80** (1998) 101–104.
[172] Mazin, I. I.; Cohen, R. E.: Insultaor-metal transition in solid hydrogen – implications for electronic structure calculations for recent experiments. Phys. Rev. **B52** (1995) R8597–R8600.
[173] Scandolo, S.; Kohanoff, J.: Optimal basis set for electronic structure calculations in periodic systems. Phys. Rev. **B62** (2000) 15499–15504.
[174] Kohanoff, J.; Scandolo, S.; Chiarotti, G. L.; Tosatti, E.; Solid molecular hydrogen: The broken symmetry phase. Phys. Rev. Lett. **78** (1997) 2783–2786.
[175] Tse, J. S.; Klug, D. D.: Evidence from molecular dynamics simulations for nonmetallic behaviour of solid hydrogen above 160 GPa. Nature **378** (1995) 595–597.
[176] Kohanoff, J.; Scandolo, S.; de Gironzoli, S.; Tosatti, E.: Dipole-quadrupole interactions and the nature of phase III of compressed hydrogen. Phys. Rev. Lett. **83** (1999) 4097–4100.
[177] Johnson, K. A.; Ashcroft, N. W.: Structure and bandgap closure in dense hydrogen. Nature **403** (2000) 632–635.
[178] Biermann, S.; Hohl, D.; Marx, D.: Proton quantum effects in high pressure hydrogen. Sol. St. Comm. **108** (1998) 337–341.
[179] Kitamura, H.; Tsuneyuki, S.; Ogitsu, T.; Miyake, T.: Quantum distribution of protons in solid molecular hydrogen at megabar pressures. Nature **404** (2000) 259–262.
[180] Pfaffenzeller, O.; Hohl, D.: Structure and electrical conductivity in fluid high-density hydrogen. J. Phys.: Condens. Matter **9** (1997) 11023–11034.
[181] Hohl, D.; Natoli, V.; Ceperley, D. M.; Martin, R. M.: Molecular dynamics in dense hydrogen. Phys. Rev. Lett. **71** (1993) 541–544.
[182] Scandolo S.: Liquid-liquid phase transition in compressed hydrogen from first-principles simulations. Proc. Natl. Acad. Sci. USA **100** (2003) 3051–3053.
[183] Loubeyre, P.; LeToullec, R.; Hausermann, D.; Hanfland, M.; Hemley, R. J.; Mao, H.-K.; Finger, L. W.: X-ray diffraction and equation of state of hydrogen at megabar pressures. Nature **383** (1996) 702–704.
[184] Nellis, W. J.; Weir, S. T.; Mitchell, A. C.: Metallization and electrical conductivity of hydrogen in Jupiter. Science **273** (1996) 936–938.
[185] Duffy, T. S.; Vos, W. L.; Zha, C. S.; Hemley, R. J.; Mao, H.-K.: Sound velocities in dense hydrogen and the interior of Jupiter. Science **263** (1994) 1590–1593.
[186] Weir, S. T.; Mitchell, A. C.; Nellis, W. J.: Metallization of fluid molecular hydrogen at 140 GPa (1.4 mbar). Phys. Rev. Lett. **76** (1996) 1860–1863.
[187] Lenosky, T. J.; Bickham, S. R.; Kress, J. D.; Collins, L. A.: Density-functional calculation of the Hugoniot of shocked liquid deuterium. Phys. Rev. **B61** (2000) 1–4.
[188] Galli, G.; Hood, R. Q.; Hazi, A. U.; Gygi, F.: *Ab initio* simulations of compressed liquid deuterium. Phys. Rev. **B61** (2000) 909–912.
[189] Collins, G. W.; Da Silva, L. B.; Celliers, P.; Gold, D. M.; Foord, M. E.; Wallace, R. J.; Ng, A.; Weber, S. V.; Budil, K. S.; Cauble, R.: Measurements of the equation of state of deuterium at the fluid insulator-metal transition. Science **281** (1998) 1178–1181.
[190] Bagnier, S.; Blottiau, P.; Clérouin, J.: Local-spin-density-approximation molecular-dynamics simulations of dense deuterium. Phys. Rev. E**63** (2002) 015301.
[191] Collins, L. A.; Bickham, S. R.; Kress, J. D.; Mazevet, S.; Lenosky, T. J.; Troullier, N. J.; Windl, W.: Dynamical and optical properties of warm dense hydrogen. Phys. Rev. **B63** (2001) 184110.
[192] Celliers, P. M.; Collins, G. W.; Da Silva, L. B.; Gold, D. M.; Cauble, R.; Wallace, R. J.; Foord, M. E.; Hammel, B. A.: Shock-induced transformation of liquid deuterium into a metallic fluid. Phys. Rev. Lett. **84** (2000) 5564–5567.
[193] Alavi, A.; Parrinello, M.; Frenkel, D.: *Ab initio* calculation of the sound velocity of dense hydrogen – implications for models of Jupiter. Science **269** (1995) 1252–1254.
[194] Pfaffenzeller, O.; Hohl, D.; Ballone, P.: Miscibility of hydrogen and helium under astronomical conditions. Phys. Rev. Lett. **74** (1995) 2599–2602.
[195] Stevenson, D.: Introduction to planetary interiors. In: *Proceedings of the International School of Physics "E. Fermi" on High Pressure Phenomena*. (Eds. Chiarotti, G.; Hemley, R.; Ulivi, L.) IOS, Amsterdam: Course CXLVII (2002) pp. 195–214.
[196] Klepeis, J. E.; Schafer, K. J.; Barbee, T. W.; Ross, M.: Hydrogen-helium mixtures at Mbar pressures: implications for Jupiter and Saturn. Science **254** (1991) 986–989.
[197] Ross, M.: The ice layer in Uranus and Neptune – diamonds in the sky. Nature **292** (1981) 435–436.
[198] Ancilotto, F.; Chiarotti, G. L.; Scandolo, S.; Tosatti, E.: Dissociation of methane into hydrocarbons at extreme (planetary) pressure and temperature. Science **275** (1997) 1288–1290.
[199] Benedetti, L. R.; Nguyen, J. H.; Caldwell, W. A.; Liu, H. J.; Kruger, M.; Jeanloz, R.: Dissociation of CH_4 at high pressures and temperatures: Diamond formation in giant planet interiors? Science **286** (1999) 100–102.

[200] Lee, C.; Vanderbilt, D.; Laasonen, K.; Car, R.; Parrinello, M.: *Ab initio* studies on high-pressure phases of ice. Phys. Rev. Lett. **69** (1992) 462–465.
[201] Benoit, M.; Bernasconi, M.; Parrinello, M.: New high-pressure phase of ice. Phys. Rev. Lett. **76** (1996) 2934–2937.
[202] Benoit, M.; Marx, D.; Parrinello, M.: Tunnelling and zero-point motion in high-pressure ice. Nature **392** (1998) 258–261.
[203] Bernasconi, M.; Silvestrelli, P. L.; Parrinello, M.: *Ab initio* infrared absorption study of the hydrogen-bond symmetrization in ice. Phys. Rev. Lett. **81** (1998) 1235–1238.
[204] Fois, E. S.; Sprik, M.; Parrinello, M.: Properties of supercritical water – an *ab initio* simulation. Chem. Phys. Lett. **223** (1994) 411–415.
[205] Boero, M.; Terakura, K.; Ikeshoji, T.; Liew, C. C.; Parrinello, M.: Water at supercritical conditions: A first principles study. J. Chem. Phys. **115** (2001) 2219–2227.
[206] Schwegler, E.; Galli, G.; Gygi, F.: Water under pressure. Phys. Rev. Lett. **84** (2000) 2429–2432.
[207] Cavazioni, C.; Chiarotti, G. L.; Scandolo, S.; Tosatti, E.; Bernasconi, M.; Parrinello, M.: Superionic and metallic states of water and ammonia at giant planet conditions. Science **283** (1999) 44–46.
[208] Chau, R.; Mitchell, A. C.; Minich, R. W.; Nellis, W. J.: Electrical conductivity of water compressed dynamically to pressures of 70–180 GPa (0.7–1.8 Mbar). J. Chem. Phys. **114** (2001) 1361–1365.
[209] Iitaka, T.; Ebisuzaki, T.: First-principles calculation of elastic properties of solid argon at high pressures. Phys. Rev. **B65** (2001) art. 012103.
[210] Savrasov, S.; Toropova, A.; Katsnelson, M. I.; Lichtenstein, A. I.; Antropov, V.; Kotliar, G.: Electronic structure and magnetic properties of solids. Z. Kristallogr. **220** (2005) 473–488.
[211] Steinle-Neumann, G.; Stixrude, L.; Cohen, R. E.; Gulseren, O.: Elasticity of iron at the temperature of the Earth's inner core. Nature **413** (2001) 57–60.